Universidad Zaragoza
1542

Final Master Project

Characterization of polycaprolactone/mesoporous silica composite membranes

Author

Iván Vera Alaya

Director

Dr. Silvia Irusta Alderete

NANOSTRUCTURED MATERIALS FOR NANOTECHNOLOGY APPLICATIONS
Institute of Nanoscience of Aragon
University of Zaragoza
2014-2015

Acknowledgements

First I would like to thank my supervisor Dr. Silvia Irusta for the opportunity to work on this research group, for their great help and patience during this project, and for the support when perform FTIR.

I would also like to thank all my lab mates and my classmates. I especially want to thank Laura López and Ismael Pellejero for their advice and for the great help they have provided me, without which it would be impossible to finish this project on time, and Ángela López for letting me use the equipment whenever I needed it for my experiments. Also deserve special attention Nuria Navascues and Carlos Cuestas for their help in making the TGA and SEM analyses.

Last but not least, I want to thank my friends, especially María Picazo for her encouragement, her understanding and her continued support throughout the course. Without her I had not started this master and, of course, I could not have been able to finish it. Many thanks “Pollo”.

Abstract

In the present project polycaprolactone (PCL) with mesoporous silica (MCM-41) as filler based membranes were prepared and characterized. PCL was chosen because it is biocompatible, biodegradable and has an excellent tensile strength. Because of these characteristics PCL has found diverse applications in several fields: packaging, tissue engineering, drug delivery, etc.

MCM-41 is a mesoporous material with hexagonal arrangement of uniform mesopores, highly specific surface (up to 1500 m^2/g), and adjustable pore diameter (2-10 nm).

Composite membranes were prepared by casting and solvent evaporation method. The inorganic loading of the membranes was measured by Thermogravimetric Analysis (TGA) while structure and morphology were analyzed by Fourier Transform Infrared Spectroscopy (FTIR) and Scanning Electron Microscope (SEM). Permeability test were carried out in a home-made experimental plant. The gases used for permeation were oxygen and carbon dioxide. Theoretical and experimental selectivity were compared.

Incorporating MCM-41 nanoparticles reduced O_2 and CO_2 permeation around 20% and 80% respectively, compared to pristine PCL. Also, incorporating these nanoparticles functionalized with EPTES caused a greater decrease in O_2 and CO_2 permeation, 26% and 90% respectively. For both composite membranes a higher O_2/CO_2 selectivity was obtained.

Table of Contents

Figures

Tables

1. Introduction

Membrane technology is one of the fastest growing fields in the last years in separation process. Even though these processes are a relatively new type of separation technology, several membranes processes, particularly pressure-driven processes including reverse osmosis, nano-filtration, ultra and microfiltration, are already applied on industrial scale **[1]**.

The concept of membrane separation process is a relatively simple process because ideally include only two flows (feed and permeate) and a separator element (membrane), as seen in Figure 1.

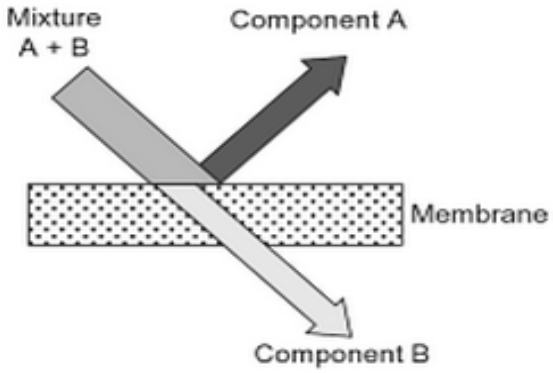

Figure 1. Basic principle of membrane process

However, the increasing complexity of separation operations makes membrane processes complex. Membrane methods are able to separate very diverse mixtures, beginning from gas mixtures containing the smallest molecules like H_2 and He, to mixtures of particles beyond molecular sizes, such as viruses or bacterial cultures. Gaseous, liquid, and supercritical media, even solids in a suspension, can be separated by membranes.

Due to this variety of substances capable of separating, membranes have found a wide application in diverse fields such as medicine, ecology, power engineering, chemical industry, agriculture, etc **[2]**.

In general, some of the main advantages of separation processes based in membranes are **[3]**:

- Separation is performed continuously
- Low energy consumption
- Easily combine with other separation processes
- Easy scale-up
- Adjustable membrane properties

Considering the structure of membranes, it can be classified into two main groups: porous and dense membranes **[4]**. Porous membranes have a highly voided structure interconnect by pores. These pores are extremely small, of the order of 0.01 to 10 microns. In this type of membranes, basically two mechanisms of gas transport occur, as shown in Figure 2. The first mechanism is based on Knudsen diffusion in which permeation is inversely proportional to molecular weight of the permeants. The other mechanism is molecular sieve where permeation is inversely proportional to the size of molecules: particles smaller than the pores will pass through the membrane, and larger particles are rejected.

In contrast, dense membranes consist of a dense film, without pores, through which permeants first dissolve in the membrane and then diffuse through it under the driving force of pressure, concentration, or potential gradient (solution-diffusion mechanism). The separation of components depends on their solution and diffusion in the membrane. Most gas separation, pervaporation, and reverse osmosis use this type of membranes.

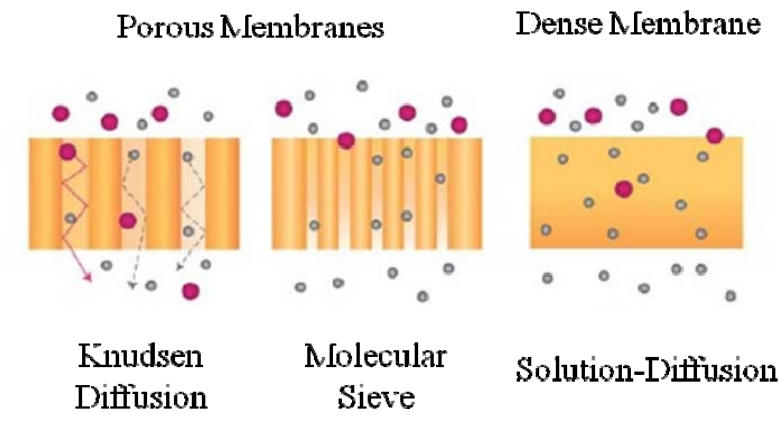

Figure 2. Types of membranes and transport mechanisms

Finally, considering the material, the membranes can be classified in organic and inorganic **[5]**. The first organic membranes were prepared from cellulose and derivatives of it, however, while still being used, it has low thermal resistance and limited resistance to chemicals. Thanks to advances in the field of synthetic polymers in recent years, these membranes of cellulose have been replaced by polymeric membranes improving quantitatively the properties. In Table 1 **[3]** the main polymers used in the manufacture of membranes is shown.

Table 1. Main polymers used in organic membranes

Polymer	MF	UF	RO	GS	PV
Cellulose and derivates	*	*	*	*	*
Polydimethylsiloxane (PDMS)				*	*
Polyethylene (PE)	*			*	
Polypropylene (PP)	*				
Polyvinyl chloride (PVC)	*	*			
Polyvinyl fluoride (PVF)	*	*			
Polymethylpentene (PMP)					*
Polyester (UP)	*				
Polyvinyl alcohol (PVA)					*
Polyacrylonitrile (PAN)	*	*	*		*
Polycarbonate (PC)	*			*	
Polytetrafluoroethylene (PTFE)	*	*			
Polyamide (PA)					*
Polyamide-imides (PAI)		*		*	
Polysulfone (PSU)	*	*	*		*
Polyether-sulfone (PES)					*
Polyphenylene oxides (PPO)			*	*	*
Polyesteramide (PEA)					*
Polybenzimidazole (PBI)		*	*		

MF: Microfiltration; UF: Ultrafiltration; RO: Reverse Osmosis; PV: Pervaporation; GS: Gas Separation

The other principal group of membranes corresponds to inorganic membranes. The use of these membranes is relatively recent and is in continuous development. This great attention from researchers is due to these membranes are more resistant mechanically, thermally and chemically than organic membranes. The most widely materials used for the manufacture of these membranes are glass, carbon, metal and ceramics, being this last material the most used.

This type of membranes consists mainly in two parts: a macroporous support, which may be flat or tubular, and different active layers which are deposited on this support, as shows Figure 3. The pore size of these supports is in the order of microns.

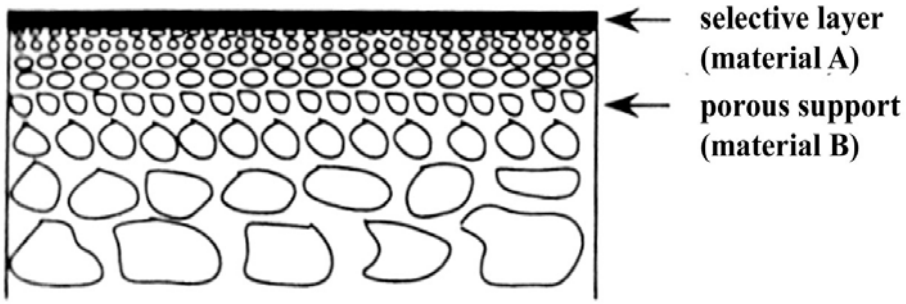

Figure 3. Scheme of the structure of inorganic membrane

Both organic and inorganic membranes present some advantages and limitation for their use in gas separation. Polymeric membranes achieve low selectivity for gas separations that involve molecules with close kinetic diameters. However these membranes are easy to manufacture with low cost and have high mechanical properties. In contrast, inorganic membranes shown exceptional gas separation properties and high stability under temperature and chemical environments, but their immediate application is still hindered by the lack of technology to form continuous and defect-free membranes, their high cost for production and their handling issues **[6-11]**.

Therefore emerges the need for innovation in this technology, and emerges a new type of membrane composed of a polymer matrix filled with inorganic particles. These membranes combine the high selectivity of inorganic membranes with the mechanical properties of polymeric membranes, obtaining new membranes suitable for separating gases, easy to manufacture and a low cost, overcoming the major drawbacks of both membranes.

From this section, this project will focus on a specific type of composite membranes formed by a polymeric matrix of poly(ε-caprolactone) (PCL) filled with MCM-41 nanoparticles as reinforcing material.

1.1. Poly(ε-caprolactone)

Poly(ε-caprolactone) (PCL) is a biodegradable polyester derived from petroleum, which is given mainly by a ring opening polymerization (ROP) of cyclic ester ε-caprolactone (Figure 4). In this polymerization reaction various types of catalysts have been used as $Sn(Oct)_2$ (Stannous octoate) **[12]** or DABCO (1,4-Diazobicyclo(2,2,2)octane) **[13]**. In this research $SnCl_2 \cdot 2H_2O$ was the catalyst used for the polymerization.

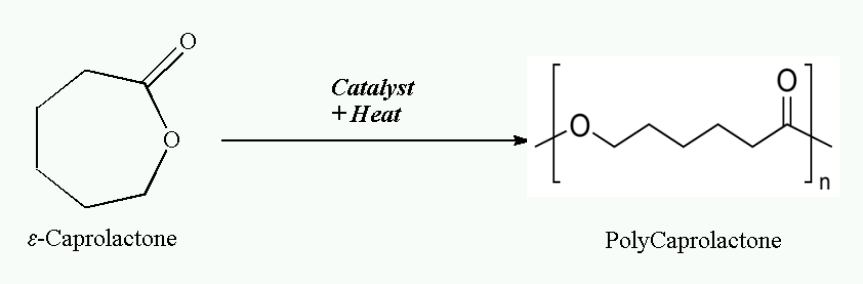

Figure 4. ROP polymerization of ε-capolactone

PCL is a semicrystalline polymer with a degree of crystallinity of 0.69 and a melting point of 60 ºC **[14]**. In addition due to its simple structure, the chains have a slight rotation, which gives a very low glass transition temperature (-72 ºC), so that at room temperature has a soft and rubbery state.

Because it is a biodegradable, biocompatible and non-toxic polymer, the PCL found in the field of biomedicine one of its main applications as devices for delivering drugs, sutures, adhesion barriers, contraceptives and even as a long term implantable biomaterial because it bioabsorbs in about two years. Besides it manufacturing is simpler than other biopolymers.

Finally also shows good barrier properties for use as gas membrane. Gorrasi et al. **[10]** established that the phenomenon of gas transport through this membranes is due

to a solution-diffusion phenomenon. In this experiment determined the solution and diffusion coefficients of for water vapor and dichloromethane. Another important parameter to determine the barrier properties of this type of membranes is the permeability. Tanaka et al. **[15]** conducted experiments on water filtration with membranes PCL. Sadeghi et al. **[9]** measured the N_2, O_2, CH_4 and CO_2 permeability in polycaprolactone based polyurethane-silica nanocomposite membrane and Gain et al. **[16]** measured the permeability of He, H_2 and CO_2 polycaprolactone/clay nanocomposites.

1.2. PCL Composites

The most widely used methods for preparing polymeric composites are: solution blending, sol-gel process and in situ polymerization **[17]**. Solution blending is the simplest method. Consist on solve the polymer in a solvent and adding the inorganic nanoparticles by stirring to achieve a good dispersion. The mixture is cast and the solvent is evaporated.

Sol-gel process is the most widely used. In this method the monomers or polymers are mixed with the nanoparticles that act as precursors for polymerization. The advantages of this method are moderated reaction conditions, easily to control the concentration and the homogeneity of the obtained membranes.

Finally in situ polymerization consist on mix the nanoparticles with the monomers which subsequently polymerized by catalysts or precursors. The biggest advantage of this method is the ability to form covalent bonds between the functional groups of the nanoparticle and the polymer chains increasing the adhesion organic matrix-inorganic filler.

PCL composites contain inorganic fillers, such as clays, silica or carbon nanotubes. Gain et al. **[16]**, Gorrasi et al. **[10]** and Lepoittevin et al. **[18]** experimented with montmorillonite (MMT) and organo-modified MMT clays filler. Cabedo et al. **[19]** used kaolitine clay as filler in a PCL/PLA blend membrane. Sanchez-Garcia et al. **[20]** research in nanobiocomposites of PCL reinforced with carbon nanofibers (CNF) and carbon nanotubes (CNT). Avella et al. **[21]** experimented with PCL-silica nanocomposites, Sadeghi et al. **[9]** with PCL based PU-silica membranes and also Lee

et al. **[22]** with PCL-silica xerogel membranes for bones regeneration. Besides these inorganic fillers, the use of organic fillers such as cellulose, starch and chitosan has also been investigated **[23-25]**.

The effects of these fillers in the nanocomposite are multiple. Lepoittevin et al. **[18]** suggested that the presence of MMT increases the mechanical properties. Besides that, the presence of fillers also affects the permeation properties. The presence of MMT clays increases the tortuosity, thereby decreasing the gas diffusion through the membrane and therefore the permeation **[10,16]**. Similar results were observed with O_2 permeation in PCL composites reinforced with CNT and CNF **[20]** and in PCL based PU membranes filled with silica **[9]**. And also the presence of silica nanoparticles increases the selectivity of the membranes.

Finally, the introduction of ordered mesoporous silica into membranes has been extensively studied to improve the permeation or selectivity **[6-8]**. Silica mesoporous nanoparticles have uniform mesopores, highly specific surface (up to 1500 m^2/g), and adjustable pore diameter (2–10 nm). These properties provide excellent interfacial adhesion with the polymer matrix. Moreover the system of internal channels allows the selective permeation of gas molecules. In addition, the possibility of additional functionalization of the silica material can further enhance sorption effects in these particles and increase gas selectivity.

2. Objectives

The main goal of this final master project was to obtain PCL/MCM-41 membranes with improved permeation properties and characterized them. The main tasks to be accomplished during the project to achieve this objective were:

- Preparation of PCL and PCL composite membranes from a polymer synthesized by the Nanostructured Films and Particles group (NFP).

- Characterization of the membranes by TGA, FTIR and SEM to check the MCM-41 loading, the structure and morphology of them.

- Perform permeation measurements of the membranes with O_2 and CO_2 and calculate the selectivities for both individual gases and mixtures.

3. Experimental Part

3.1. Material

3.1.1. Synthesis of MCM-41

The synthesis of MCM-41 was carried out by a hydrothermal synthesis **[26]** which requires three reactive (see Figure 5): CTAB (cetyltrimethylammonium bromide, $C_{16}H_{33}N(CH_3)_3Br$, ≥99%), that acts as template agent, NaOH (pellets, ≥98%) to achieve basic pH, and TEOS (tetraethyl orthosilicate, $Si(C_2H_5O)_4$, 98%), the silicon source. These three reagents were purchased from Sigma-Aldrich.

For this synthesis, 2 g of CTAB were first dissolved in 2000 mL of deionized water and then 14 mL of NaOH solution (2 M) were added, and the solution was stirred for 30 minutes at room temperature. After this time, 10 mL of TEOS were added and stirred for 3 hours at 80 ºC. Finally the solution was vacuum assisted filtered and the solid sample was calcined at 550 ºC for 5 h following a heating rate of 5 ºC/min to remove the template and to obtain the porous MCM-41.

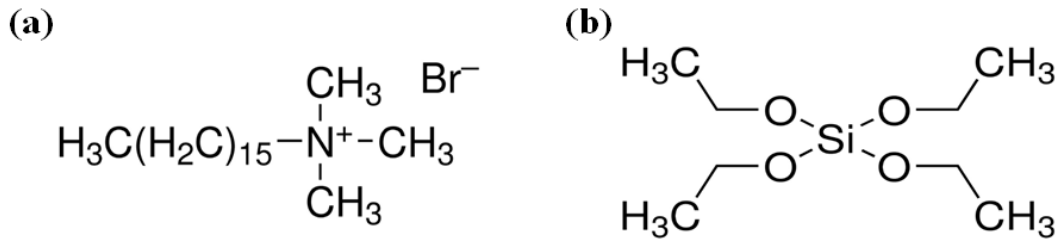

Figure 5. Structure of CTAB (a) and TEOS (b)

3.1.2. Functionalization of MCM-41

The procedure to carry out the MCM-41 functionalization with amino groups was performed by add 0.25 g of MCM-41 into a three-neck flask with cooling under Argon (99.999%) atmosphere. Then 10 mL of anhydrous toluene (99.8%, Sigma-Aldrich) were added and the mixture was stirred for 30 min. After this time, the solution was heated to 120 ºC and 0.15 mL of EPTES ([3-2-Aminoethylamino)propyl]

trimethoxysilane, $C_8H_{22}N_2O_3Si$, ≥80%, Sigma-Aldrich), Figure 6, were added and stirred for 3.5 h.

Finally, the solution was cooled at room temperature, filtered under vacuum and washed several times with toluene (≥99.5%, Sigma-Aldrich) to recover the solid.

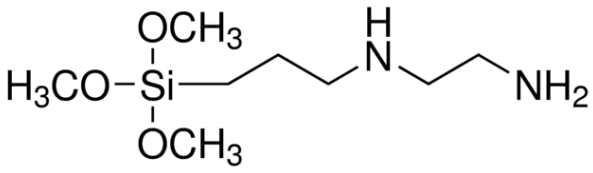

Figure 6. Structure of EPTES

3.1.3. Synthesis of PCL and PCL composites

PCL and PCL composites were produced by Nanostructured Films and Particles group (NFP) at the Institute of Nanoscience of Aragon (INA) by in situ polymerization of ε-caprolactone monomer (97%, Sigma-Aldrich) using $SnCl_2 \cdot 2H_2O$ (98%, Sigma-Aldrich) as catalyst **[27]**.

Three samples of PCL were used in this project: pristine PCL, PCL filled with 1.74% wt of MCM-41 (PCL-MCM) and PCL filled with 2.01% wt of MCM-41 functionalized with EPTES (PCL-MCM-EPTES).

Tasks 2.1.1 to 2.1.3 were carried out by other members of the NFP group.

3.2. Preparation of PCL membrane

PCL membranes were produced by solution casting and solvent evaporation method **[28]**. First, 0.75 g of solid PCL was placed in an oil bath at 80 ºC 5 minutes to facilitate dissolution. Then 20 mL of chloroform were added and the solution was stirred at 300 rpm during 27 minutes. After this time the solution was cooled with wet paper for 2 min. Finally the solution was cast on a Teflon caster (Figure 7) and the solvent was evaporated (in a hood) at room temperature for 24 hours. PCL composite membranes were prepared by the same method using the PCL with fillers as raw material.

Figure 7. Teflon caster

Membranes were cut to the appropriate size to fit in the permeation module, which in this case was 25 mm in diameter, as shown in Figure 8. Thickness of the membranes were measured with a micrometer (Baxlo 4000), obtaining an average of 60 μm.

Figure 8. Membrane samples: (a) Membrane after the casting process and (b) Membrane with the optimized size for the permeation measurements

3.3. Thermogravimetric Characterization

The degradation temperature of PCL and PCL composites, and the amount of silica in the polymer were evaluated by Thermal Gravimetric Analysis (TGA) using an Universal Analysis Q5000 instrument. Samples were placed in a platinum melting cup

and TG analyses were carried out at a rate of 5 °C/min from 30 to 800°C under N_2 atmosphere. The amount of filler dispersed in PCL membrane was calculated from the remaining mass. MCM-41 and MCM-41 functionalized powders were also analyzed in the same conditions.

3.4. FTIR Characterization

PCL and PCL composites were analyzed by FTIR spectroscopy (Vertex 70 spectrometer) in the 4000-600 cm^{-1} region. The number of scans was fixed to 40 with a resolution of 4 cm^{-1}. MCM-41 and MCM-41 functionalized powders were also analyzed in the same conditions.

3.5. Scanning Electron Microscope Characterization

The morphology of the membranes and the distribution of silica particles were examined using Scanning Electron Microscopy (SEM), FEI Inspect F50. In order to improve image resolution, all samples were coated with a 15 nm platinum layer deposited by sputtering (SC7620 Mini Sputter Coater, Quorum Technologies) to minimize electron damage to the sample, electron beam voltage was fixed at 10 kV maximum.

3.6. Permeation Characterization

3.6.1. Equipment

Permeation experiments were carried out in an home-made experimental plant, which scheme is depicted in Figure 9. The plant was controlled by a software (based in labView® and developed by electronic instrumentation service of University of Zaragoza) that allowed modify mass flow controllers (MFC), and a system of electrovalves (EV) to select the appropriate gas feeds for membrane experiments. O_2 and CO_2 (99.99% and 99.999% respectively) feed mixtures the permeation module and He (99.9%) was used as a carrier. Permeate and retentate are selected alternativately

(manual valves V1 and V2) and carry to a gas analyzer (Micro gas chromatograph) for quantification.

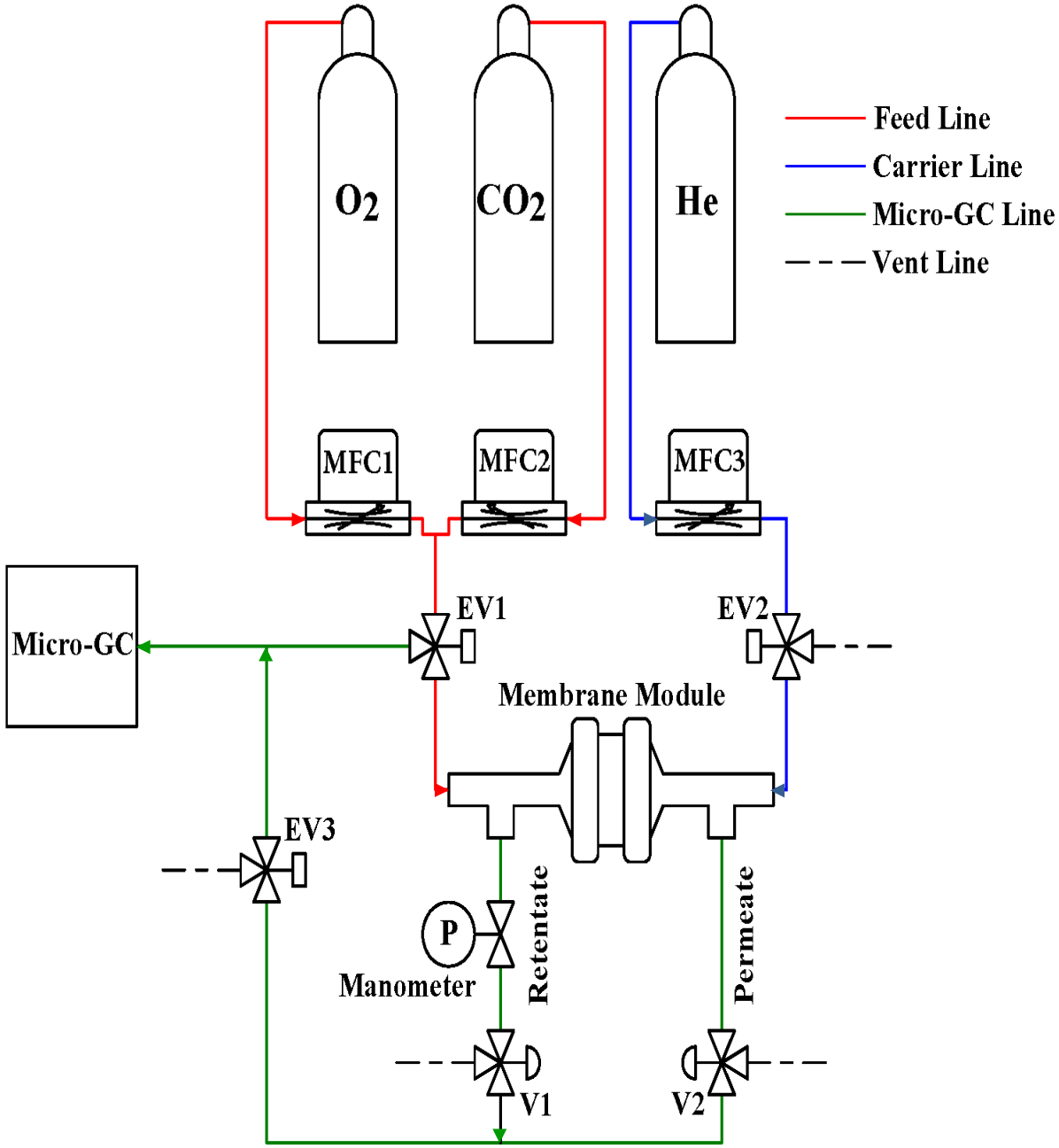

Figure 9. Scheme of the permeation plant

Membrane module (Pall Corporation PN1209) is shown in Figure 10: the membrane was placed on a metal grid inside the module and by an o-ring was achieved to remained it sealed.

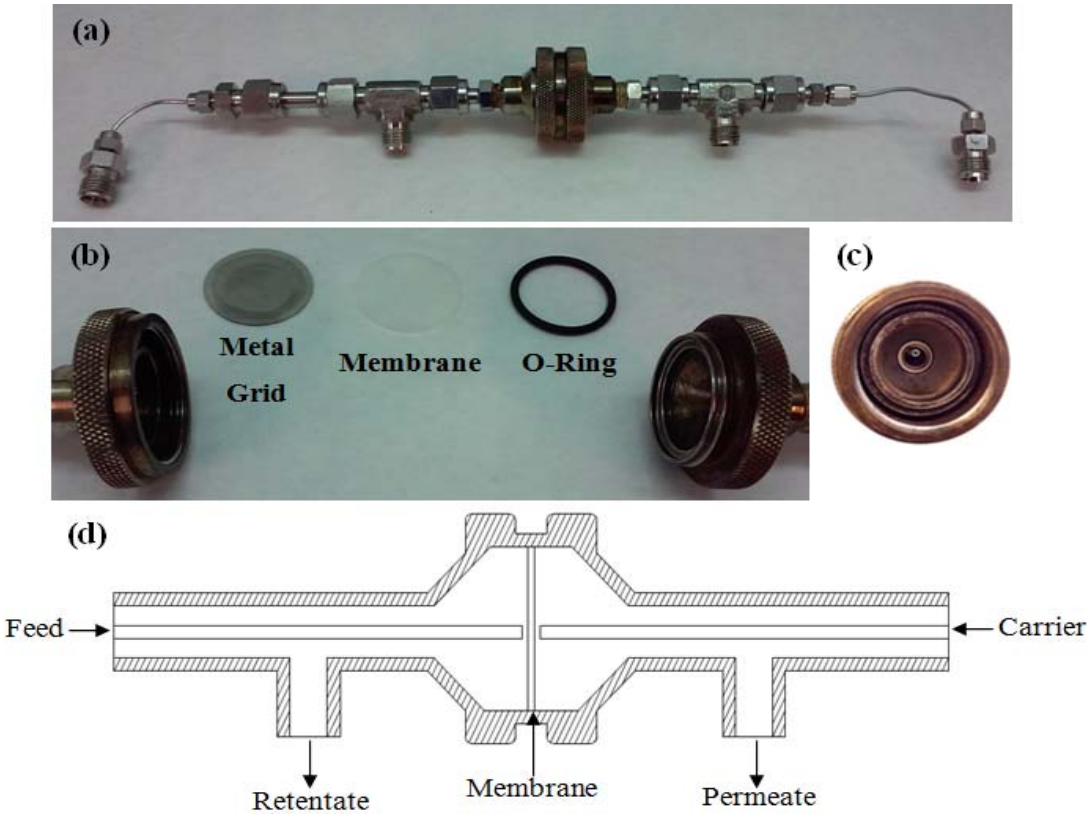

Figure 10. Permeation module. (a) Side view (b) Position of the components (c) Inner side view (d) Scheme of the module

As seen in the Figure 10.d, this module consists in two concentric tubes through which gases circulate. The inlet gases, feed and carrier, flow through the inner tube, and the exit gases, permeate and retentate, on the outside.

Finally, after passing through the system gases were analyzed using a Variant CP-4900 Micro-gas chromatograph equipped with two columns, a molecular sieve (Molsieve 5A) to separate O_2 and N_2 in this case, and a PoraPlot Q (PPQ 10) column to quantify CO_2.

Table 2 shows the conditions of temperature and pressure used for the analysis of the two columns.

Table 2. Conditions of the columns

	Channel A (Molsieve 5Ă)	Channel B (PPQ 10)
Column Temperature (ºC)	70	60
Injector Temperature (ºC)	110	110
Pressure (kPa)	120	100

3.6.2. Permeation Measurement

3.6.2.1. Calibration of the equipment

Before using the equipment, calibration of mass flow controllers and the micro gas chromatograph was performed. First, flow controllers were calibrated, for this purpose the gauges were open to different apertures and the flow was measured with a bubblemeter to obtain a calibration line: flow (mL/min) vs. % aperture.

The micro gas chromatograph was calibrated similarly measuring known concentrations of gases to obtain a relationship between the peak areas measured and the gas concentration.

3.6.2.2. Membrane Stabilization

In order to get good peak resolution it was necessary column regeneration. For regeneration procedure columns were kept at 250 ºC for 24 h to ensure that any gas which could affect the measurements was eluded from the system.

After completing this process, a membrane was placed on the support and the system was stabilized with a mixture of 20 mL/min of O_2 or CO_2 and 20 mL/min of He for 30 minutes to remove any gas that may remain in the pipes or in the membrane module.

In order to check the absence of pores or defects in the membrane, during the stabilization time, the pressure in the retentate line was increased up to 0.5 bar. It was found that with defective membranes it was not possible to achieve this pressure.

Further analysis of these membranes by SEM revealed the presence of pores and holes, as shown in Figure 11.

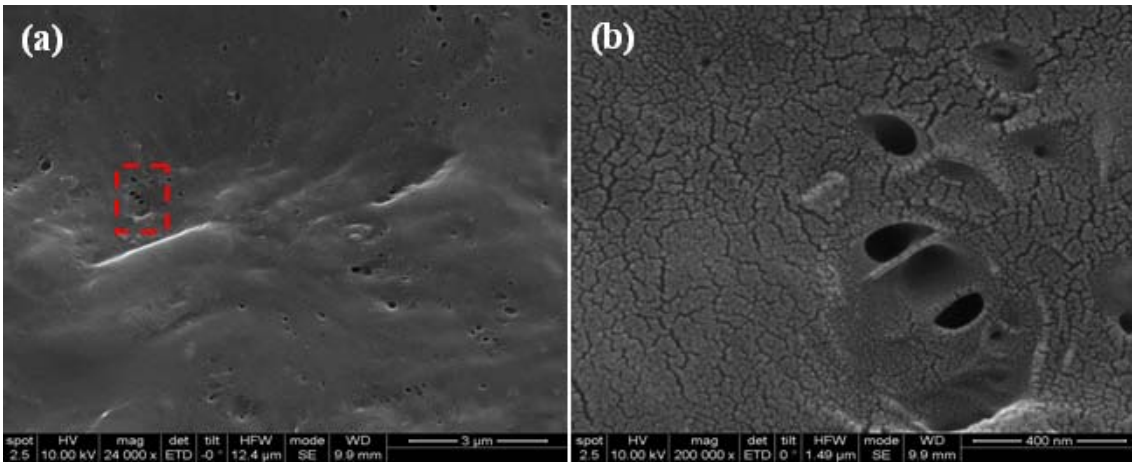

Figure 11. Membrane with defects (a) and enlargement of the marked zone (b)

3.6.2.3. Permeate, Retentate and Feed Measurement

A feed gas flow, 50 mL/min of O_2, CO_2, or mixtures of these gases, were introduced to the membrane module through the retentate side, and the same flow of carrier, He, for the permeate side. The position of the manual valve allowed the selection of the retained or permeated.

Furthermore, through the system of valves was possible to send the feed directly to the chromatograph without passing through the membrane to check the feed composition and close the mass balance.

All gas flows (retentate, permeate, feed and carrier) were measured using a bubblemeter in each experiment for subsequent calculations and also to check that there was no leakage in the system.

All measurements were performed at atmospheric pressure and with 1.5 bar. Due to the thickness of the membrane (60 µm), it was found that pressures higher than 0.75 bar just breaking membranes, as shown in Figure 12.

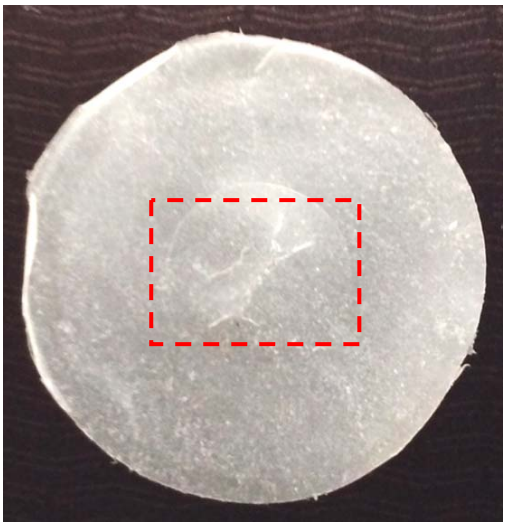

Figure 12. Membrane cracks after permeation measurements

3.6.2.4. Permeation Calculation

Permeability of the membranes was calculated by Equation 1, where P is permeability (mol·m·s^{-1}·m^{-2}·Pa^{-1}), F is the molar flux of gas (mol/s) which flows through an effective membrane area (A [m^2]) with a determinate thickness (e [m]), under a partial pressure gradient across the membrane (ΔP [Pa]) **[29]**.

$$P = \frac{F \cdot e}{A \cdot \Delta P_{al}} \qquad \textit{(Equation 1)}$$

The pressure gradient used was calculated as an average logarithmic pressure difference as shown in Equation 2 using partial pressures of each interest gasses (O_2 and CO_2).

$$\Delta P_{al} = \frac{\Delta P_1 - \Delta P_0}{ln\frac{\Delta P_1}{\Delta P_0}} \qquad \textit{(Equation 2)}$$

$$\Delta P_0 = P_{retentate} - P_{permeate} \qquad \textit{(Equation 3)}$$

$$\Delta P_1 = P_{feed} - P_{carrier} \qquad \textit{(Equation 4)}$$

Operating conveniently Equation 2, and taking into account that the total pressure of the feed is the same as the total pressure of the retentate, and the partial pressure in the carrier is zero (in this flow there is only He), the following equation is obtained based on mole fractions.

$$\Delta P_{al} = \frac{P_{ret}\left(X_{ret} - X_{feed}\right) - P_{perm} \cdot X_{perm}}{ln\frac{P_{ret} \cdot X_{ret} - P_{perm} \cdot X_{perm}}{P_{ret} \cdot X_{alim}}} \quad \textit{(Equation 5)}$$

To facilitate comparison among measurements and also with the literature, and to avoid very small numbers, the unit used in this work is the Barrer **[30]**.

$$1\ Barrer = \ 3.348 \cdot 10^{-16}\frac{mol \cdot m}{m^2 \cdot s \cdot Pa} \quad \textit{(Equation 6)}$$

Finally, selectivity, of the membranes was calculated from the gas permeation as shown in Equation 7.

$$S_{O_2/CO_2} = \frac{(P_{O_2})_{Permeate}}{(P_{CO_2})_{Permeate}} \quad \textit{(Equation 7)}$$

4. Results and Discussion

4.1. Thermogravimetric Characterization

The thermal stability of PCL and PCL composite membranes was studied using TGA. Figure 13 shows the weight loss for each membrane vs. temperature. As can be seen, membrane decomposition starts at 250 ºC. At temperature higher of 400 °C the polymer was completely decomposed. In the nanocomposites membranes the final residue was less than 2 wt %. The membrane with MCM-41 presented around 1.35% and the membrane with functionalized MCM-41 1.4%, which corresponded to the amount of filler in each membrane.

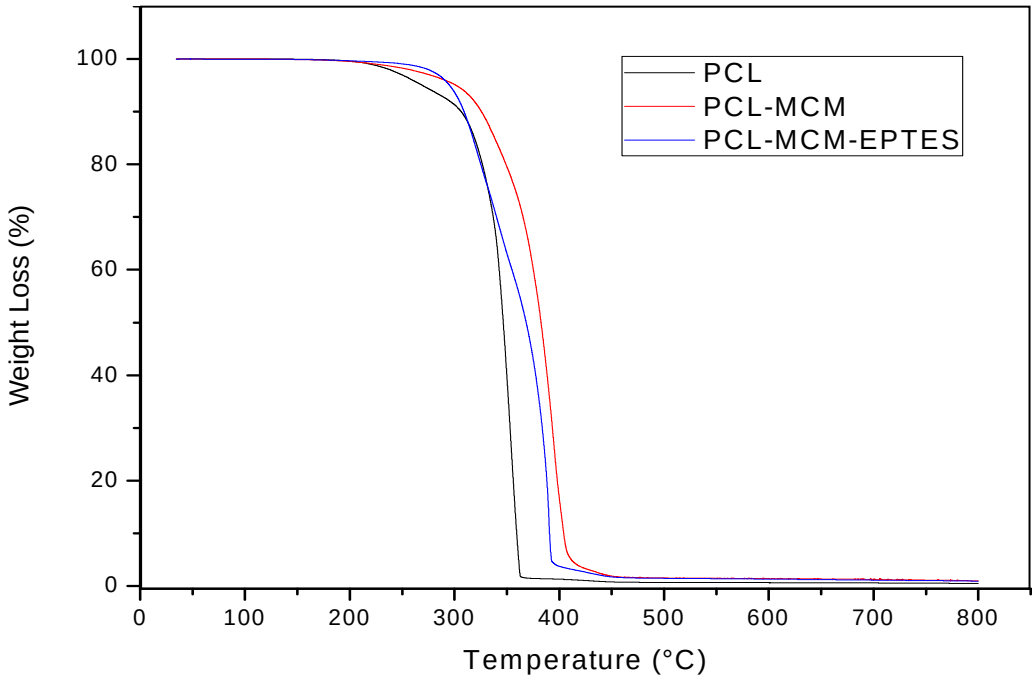

Figure 13. TGA analysis of the membranes

Representing the derivative weight loss as a function of temperature Figure 14 is obtained, which allows to clearly see the variation in degradation temperature.

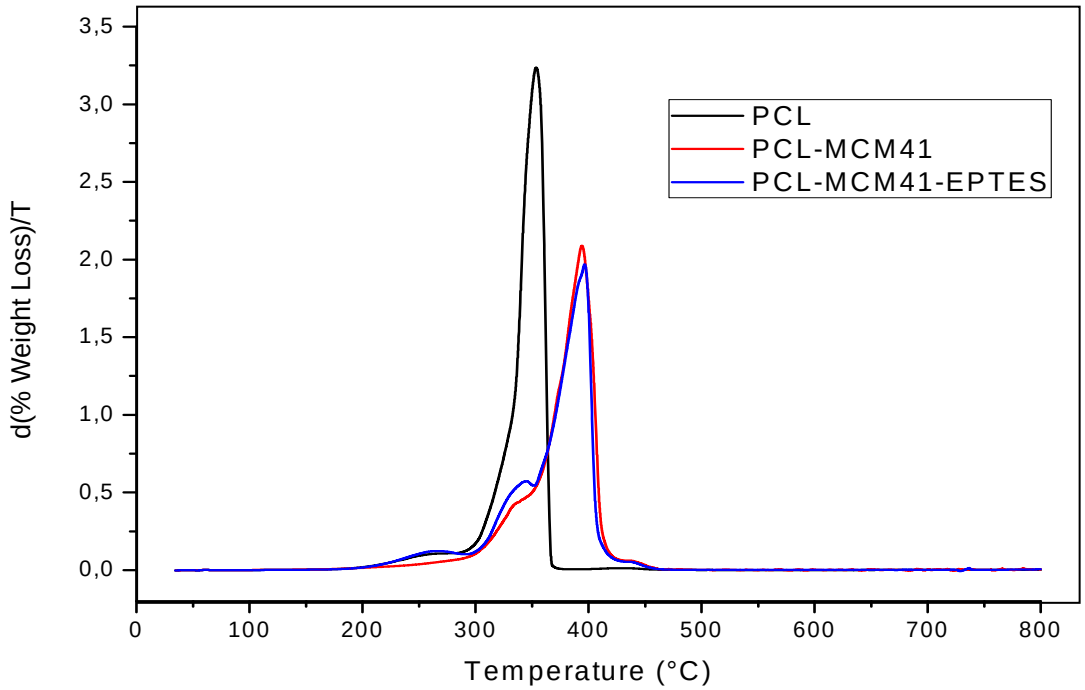

Figure 14. Degradation temperature of the membranes

The presence of filler in the membrane increased the degradation temperature by around 50 ºC. This increment in thermal stability was due to the interaction of silica particles with the polymer matrix **[31]**. In this case, two main interactions have occurred: polymer chains occluded the pores of the silica, and hydrogen bonds were performed between the carbonyl group of the polymer and silanol groups of the silica **[32]**. Both interactions contribute to decrease the mobility of the polymer chains, increasing the rigidity of the composite and thereby increasing the degradation temperature. A summary of TGA analysis data is shown in Table 3.

Table 3. Results of the TGA analysis

Sample	Inorganic Content (%wt)	Degradation Temperature (ºC)
PCL	0	355 ± 3.66
PCL-MCM41	1.34 ± 0.42	393 ± 1.70
PCL-MCM41-EPTES	1.41 ± 0.53	398 ± 1.36

Furthermore this technique was used to analyze both fillers. Results are shown in Figures 15 and 16.

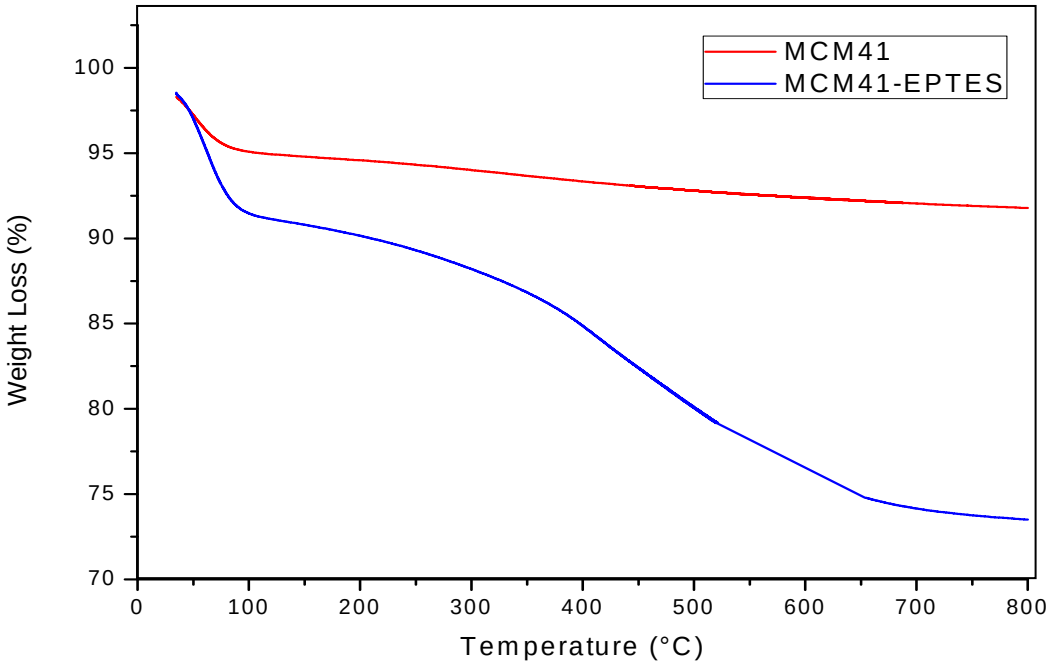

Figure 15. TGA analysis of the fillers

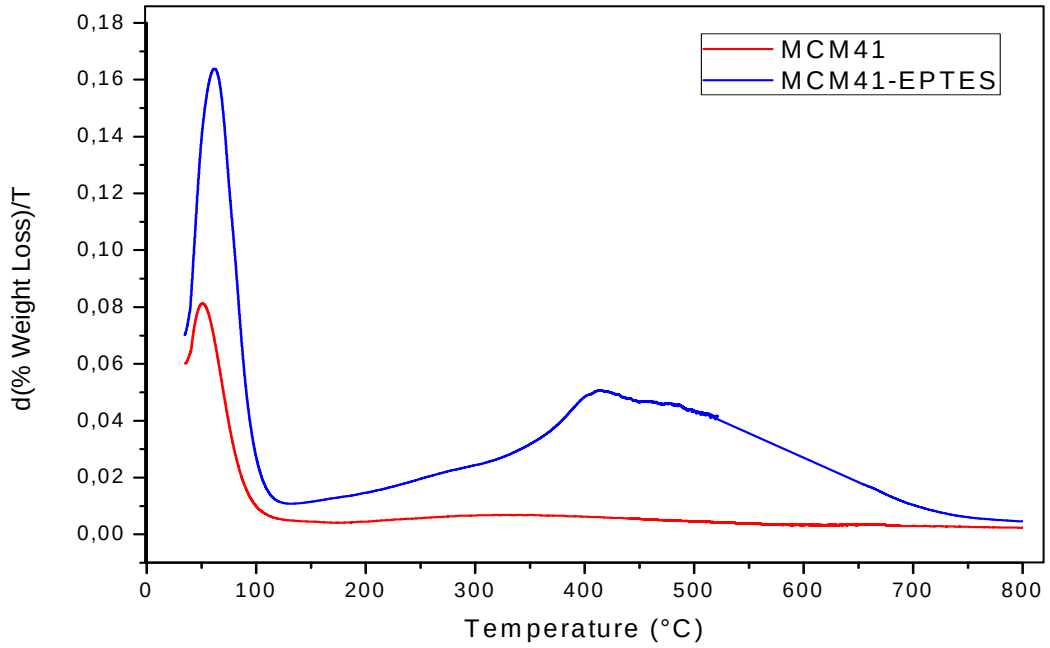

Figure 16. Degradation temperature of the fillers

Both fillers show a weight loss around 100 °C corresponding to the water removal. Furthermore, MCM-41 functionalized with EPTES showed a second weight loss around 450 °C corresponding to EPTES degradation. In Figure 15 is observed that in this second slope the weight loss was approximately 17 %, corresponding to the percentage of functionalization of MCM-41.

4.2. FTIR Characterization

The chemical structure of PCL is shown in Figure 17. The spectra show a strong peak at 1727 cm^{-1} which is assigned to carbonyl group in polycaprolactone. Another peak of interest is the 1190 cm^{-1} corresponding to O=C-O bond, which together with the previous one are the two main bonds of polycaprolactone. Finally, peaks at 2950 and 2865 cm^{-1}, correspond to CH_2 groups **[33]**. The peaks of interest indicated in Figure 17 are tabulated in Table 4.

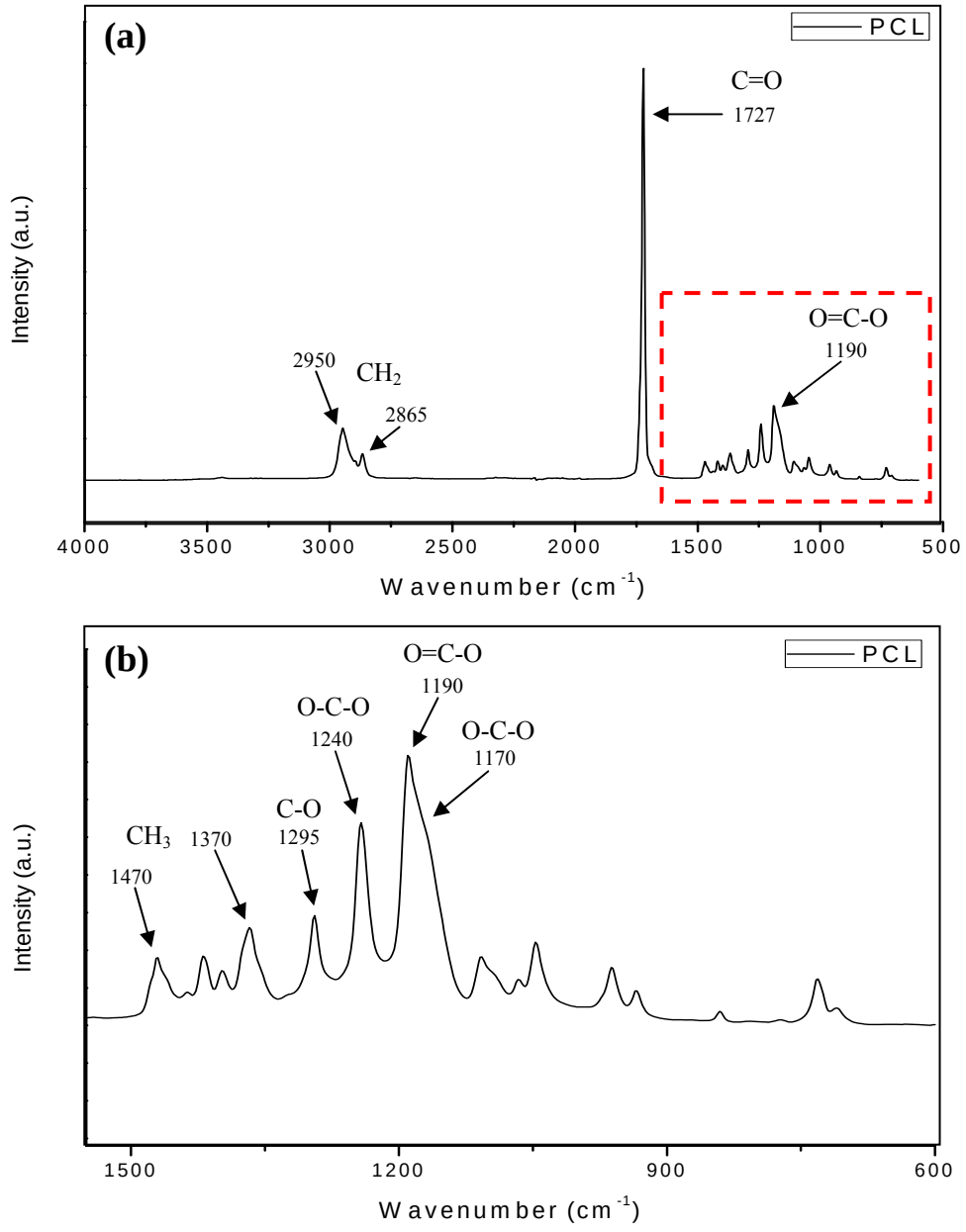

Figure 17. FITR spectra of PCL: (a) Complete frequency range and (b) Low frequency range

Table 4. Characteristic infrared bands of PCL

Position (cm^{-1})	Vibrator
2950	Asymmetric CH_2 stretching
2865	Symmetric CH_2 stretching
1727	C=O stretching
1470	Asymmetric CH_3 stretching
1370	Symmetric CH_3 stretching
1295	C-O and C-C stretching
1240	Asymmetric COC stretching
1190	O=C-O stretching
1170	Symmetric COC stretching

By this technique both fillers, MCM-41 and MCM-41 functionalized with EPTES were also analyzed, and the spectra are shown in Figures 18 and 19 respectively.

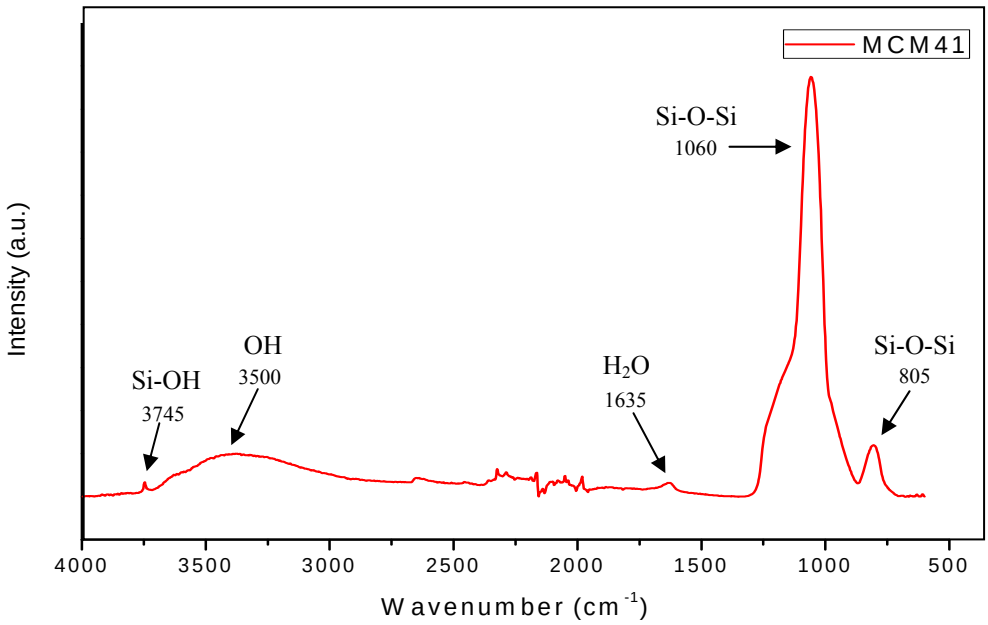

Figure 18. FTIR spectrum of MCM-41

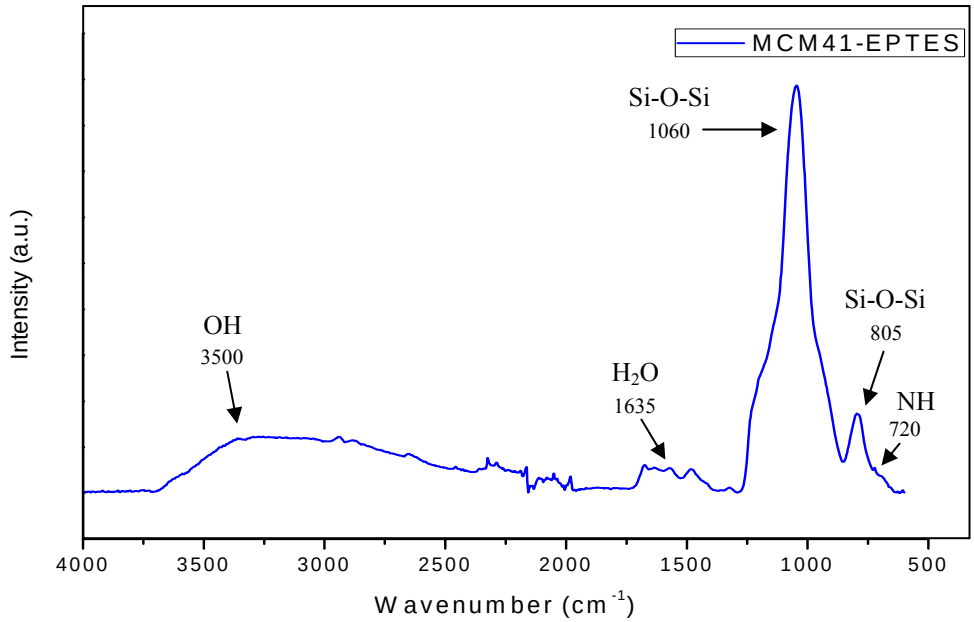

Figure 19. FTIR spectrum of MCM-41 functionalized with EPTES

The peak assignation is show in Table 5. As can be seen both spectra show two strong peaks at 1060 and 805 cm^{-1} which are assigned to Si-O-Si bonds, the most characteristic groups of MCM-41. Another peak of interest appears at 1635 cm^{-1}, which is assigned to adsorbed H_2O **[34]**. The presence of this peak indicates that the non-functionalized MCM-41 contain water despite having been calcinated, which indicates that the silica framework is hydrophilic. The broad band around 3500 cm^{-1} corresponds with hydroxyl groups in the external and internal structure which confirms the hydrophilicity of the silica **[35]**. The small shoulder in Figure 19 at 720 cm^{-1} corresponds to NH group present in the EPTES.

Table 5. Characteristic infrared bands of MCM-41 and MCM-41 functionalized with EPTES

Position (cm^{-1})	Vibrator
3745	Free silanol groups
3500	Hydroxyl groups
1635	Stretching mode of H_2O
1060	Asymmetric Si-O-Si stretching
805	Symmetric Si-O-Si stretching
720	NH bending

Another difference between the filler spectra can be seen in the regions of 2700-3000 cm^{-1} and 1300-1500 cm^{-1} as shown in Figure 20.

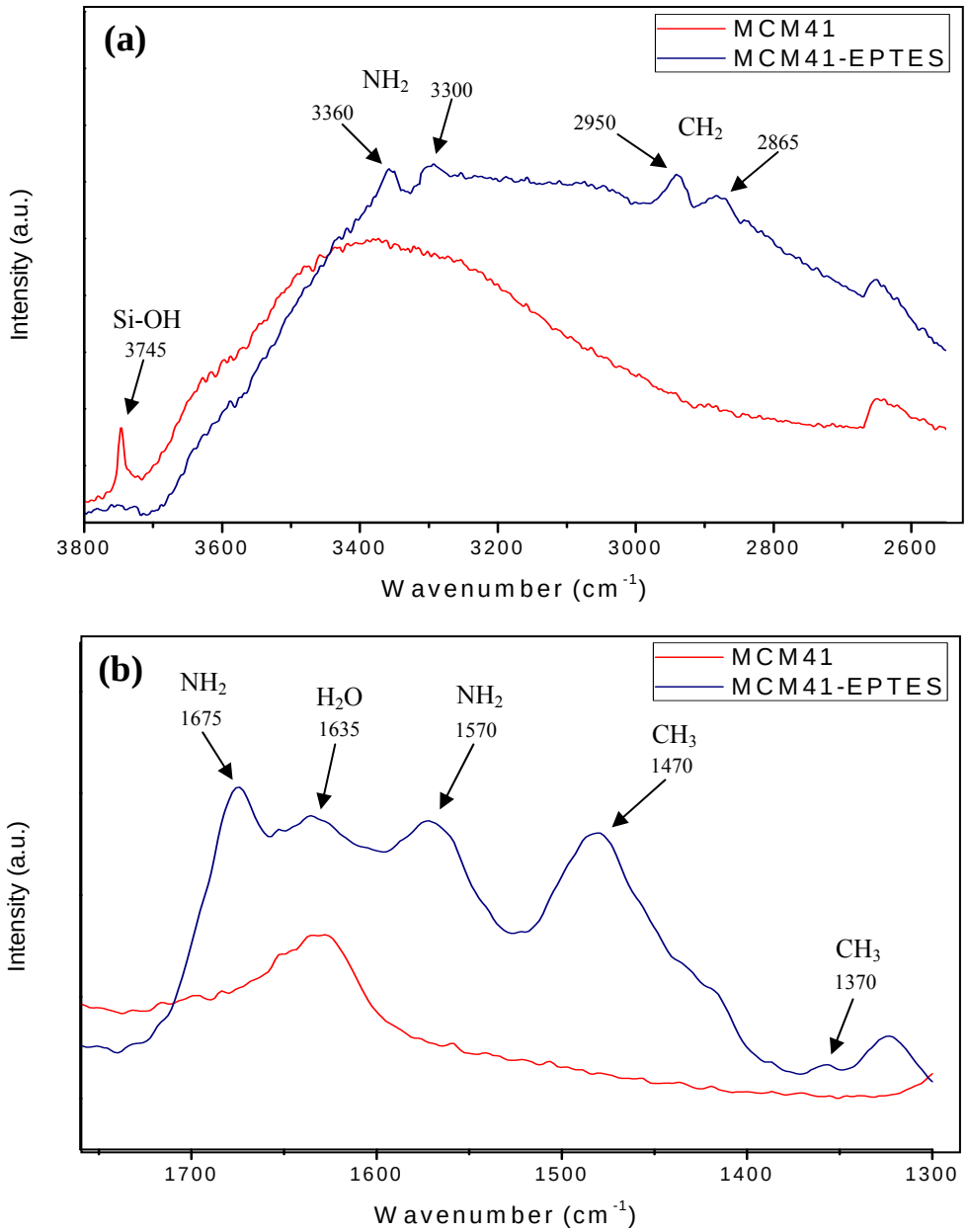

Figure 20. FTIR spectra of fillers in the high (a) and low (b) frequency range

In the case of non-functionalized MCM-41 no bands were observed in those intervals. Bands related to carbon-hydrogen bonds appears in those ranges, it suggests that the template has been completely removed during the calcination of the samples **[36]**.

The spectrum of EPTES functionalized MCM-41 shows peaks corresponding to CH_2 (2950 and 2865 cm^{-1}) and CH_3 (1470 and 1370 cm^{-1}) groups. In addition to these

peaks, there are four peaks corresponding to the NH_2 groups introduced by EPTES at 3360, 3300, 1675 and 1570 cm^{-1}. Finally another important difference between both spectra is the peak at 3745 cm^{-1} corresponding to free silanol groups. The absence of this peak in the functionalized silica confirms that the amine groups of the EPTES are bonded to free silanol groups during functionalization step. These peaks together with the peaks corresponding to NH_2 groups confirm the functionalization of the silica **[37-38]**. The peaks of interest indicated in Figure 20 are tabulated in Table 6.

Table 6. FTIR bands related EPTES

Position (cm^{-1})	Vibrator
3745	Free silanol groups
3360	Asymmetric NH_2 stretching
3300	Symmetric NH_2 stretching
2950	Asymmetric CH_2 stretching
2865	Symmetric CH_2 stretching
1675	Deformation mode of NH_2
1635	Stretching mode of H_2O
1570	NH_2 bending
1470	Asymmetric CH_3 stretching
1370	Symmetric CH_3 stretching

4.3. Scanning Electron Microscope Characterization

The morphology of the membranes of both PCL and PCL composite were analyzed by SEM. This technique was also useful to confirm the presence of silica nanoparticles. Finally using Energy-Dispersive X-ray spectroscopy (EDX) the composition of both particles membranes were analyzed.

First PCL pristine membrane was measured to use as a control membrane. Different points of the sample were analyzed in order to check the homogeneity of the membrane and the absence of defects. Results are shown in Figure 21.

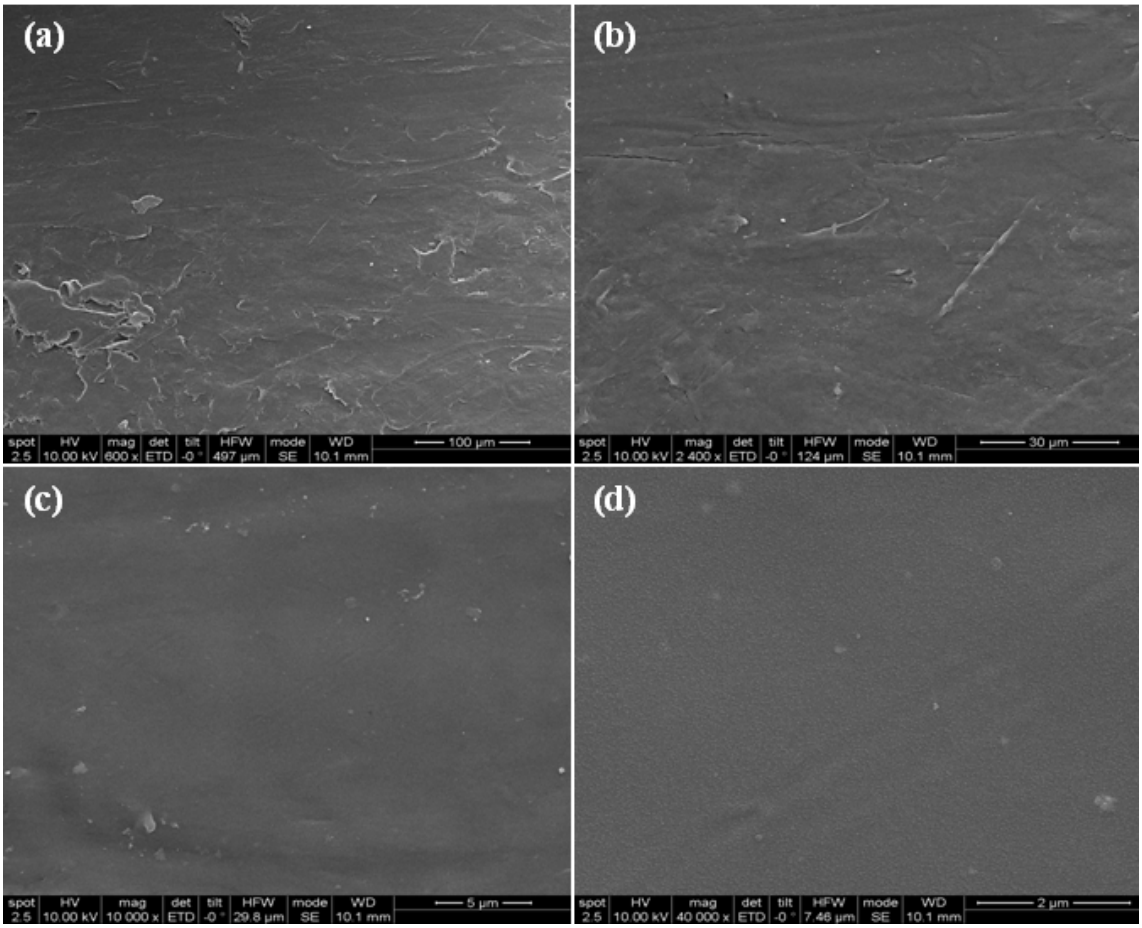

Figure 21. SEM images of pristine PCL membrane at different magnifications

As seen in Figures 21a and 21b, PCL pristine membrane is not completely flat but has a certain surface roughness. This roughness is due to its preparation by the casting process. However at higher magnification, Figure 21c and 21d, it can be seen that the membrane has high homogeneity and no defects such as pores or holes.

In order to check the composition of the membrane, and the absence of impurities, several EDX analysis of the area shown in Figure 21d were performed. This area was chosen because there are shapes that seem small particles. After analysis by EDX, it was confirmed that these shapes are areas where the polymer is not completely flat, resulting in those forms which are easily confused with particles or impurities.

Due to the conditions used: spot 2.5 and a voltage of 10kV, the electron beam is capable of penetrating a depth of about 1.3 micron so both the silica nanoparticle and the polymer beneath were analyzed to determine the composition of the membranes.

The results of these analyses are shown in Table 7. A summary of results obtained from each point marked in the figure in weight %, and an average with standard deviation are shown.

Table 7. EDX results of a pristine PCL membrane

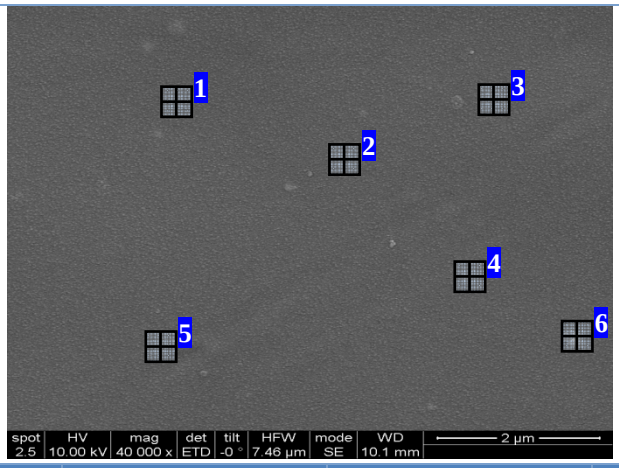

Spectrum	C	O	Si
1	74.16	25.84	-
2	77.04	22.96	-
3	73.77	26.23	-
4	76.43	23.57	-
5	75.28	24.72	-
6	73.21	26.79	-
Mean	**74.98 ± 1.53**	**25.02 ± 1.53**	-

As seen in Table 7, this membrane contains only carbon and oxygen in a proportion of 75 and 25% respectively. As mentioned above, those results confirm the absence of impurities in the membrane.

In Figure 22, images of PCL membrane with MCM-41 are shown. These membranes have a similar PCL pristine membrane homogeneity, with no pores and defects, confirming that the introduction of MCM-41 does not change the homogeneity of the membranes. Additionally as shown in Figure 22a, no aggregation of the silica nanoparticles was observed. Grainy surface, seen in Figure 22b is due to the platinum coating.

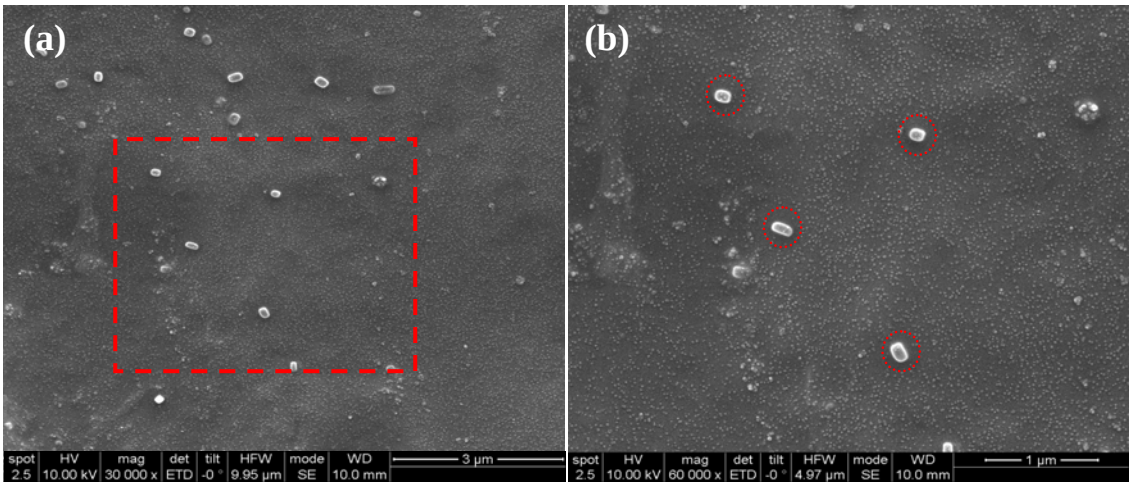

Figure 22. SEM images of PCL-MCM41 (a) and magnification of the marked zone (b)

Without high magnification it is possible to see the silica particles. Due to the method of preparing the membranes, it is possible that most of these nanoparticles are dispersed in the surface of the membrane.

As long as these experiments were performed a large number of particles were measured as shown in Figure 23. After analyzing these measurements can be concluded that the particles used in this project have a rectangular shape with an average dimensions of 150 x 90 nm.

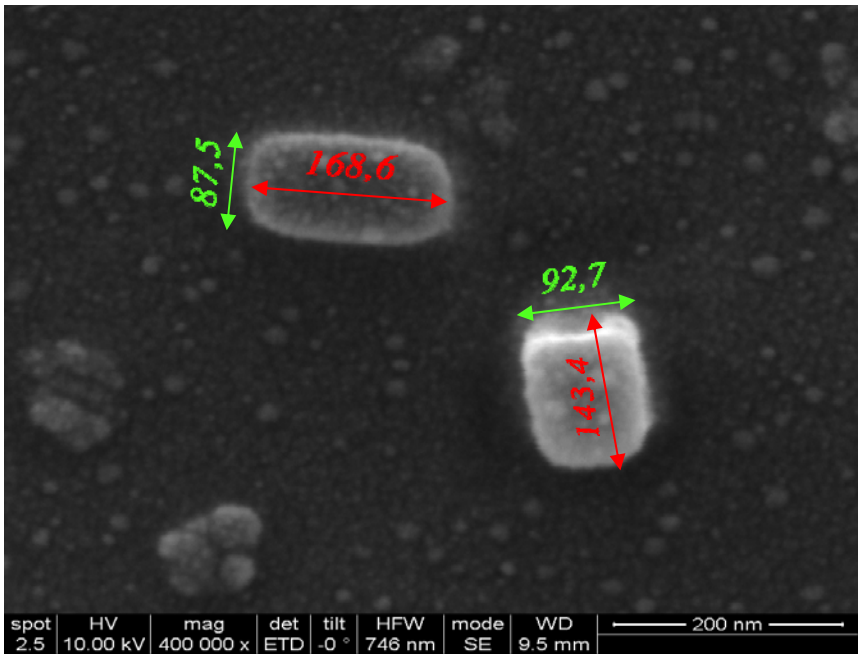

Figure 23. Detail of the MCM-41 nanoparticles

As in the case of pristine PCL, these membranes were also analyzed by EDX on the area shown in figure 22a. The results of this analysis are shown in Table 8.

Table 8. EDX results of a PCL-MCM41 membrane

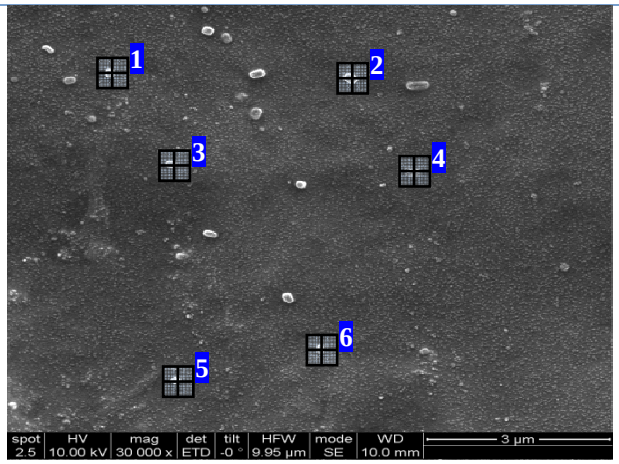

Spectrum	C	O	Si
1	64.29	32.69	3.02
2	62.69	34.97	2.34
3	63.10	33.43	3.47
4	61.06	35.81	3.13
5	65.71	31.57	2.72
6	61.48	35.68	2.84
Mean	**63.06 ± 1.74**	**34.03 ± 1.73**	**2.92 ± 0.38**

As can be seen, the results in Table 8 confirm the presence of silica. The MCM-41 concentration in the membranes used was 2%, so the fact that the EDX analysis shows a concentration around 3%, suggest that these nanoparticles are slightly concentrated on the surface of the membrane.

Finally, a difference in the percentage of oxygen compared to the membrane of pristine PCL (≈ 25%) is observed. This increase in oxygen percentage could be due to oxygen present in the MCM-41 structure.

Figure 24 shows images of PCL membranes with MCM-41 functionalized with EPTES. As in the previous case, no defects were observed in the membrane.

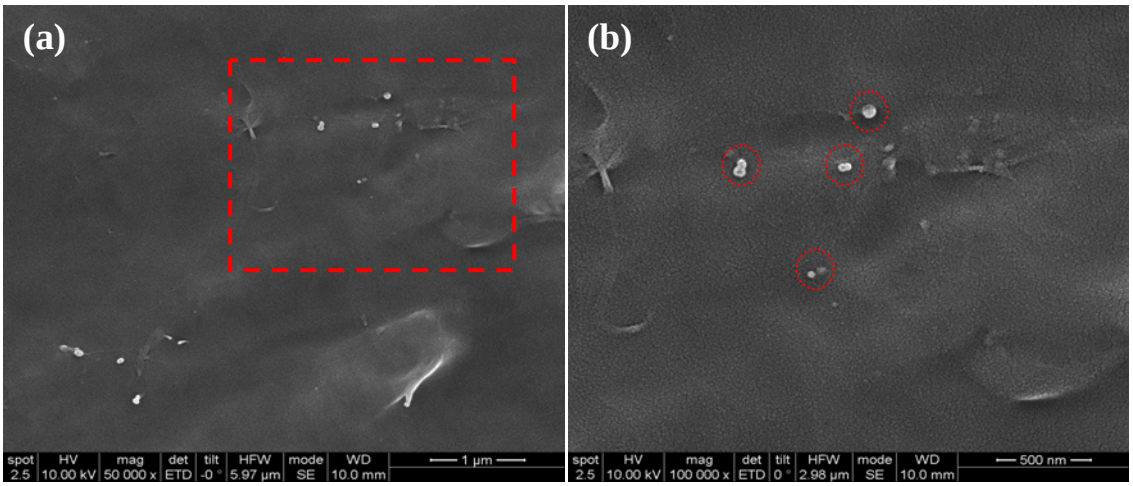

Figure 24. SEM images of PCL-MCM41-EPTES (a) and magnification of the marked zone (b)

As seen in Figure 24, these particles show similar shape and size compared with the non functionalized MCM-41. However, a greater dispersion in the case of the functionalized particles was observed, probably due to the good interaction between EPTES and polymer. Table 9 shows the results of EDX analysis of the displayed image area at Figure 24a, showing a similar composition than the previous one.

Table 9. EDX results of a PCL-MCM41-EPTES membrane

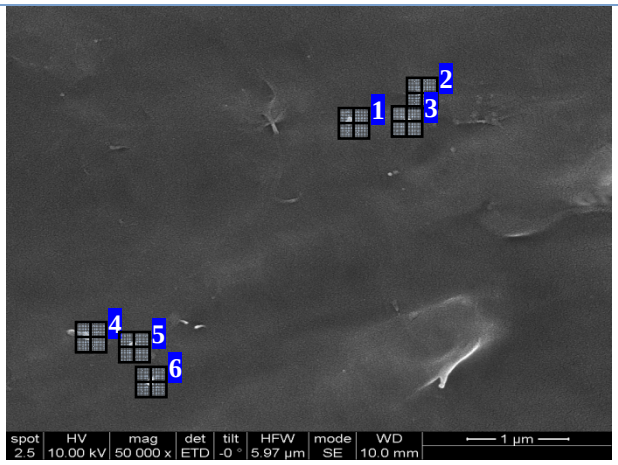

Spectrum	C	O	Si
1	66.24	30.95	2.81
2	64.63	32.25	3.12
3	63.05	33.65	3.30
4	65.82	31.34	2.84
5	67.58	29.67	2.75
6	64.37	32.66	2.97
Mean	**65.28 ± 1.60**	**31.75 ± 1.40**	**2.97 ± 0.21**

4.4. Permeation Characterization

O_2 and CO_2 permeation of composite membranes was measured by the experimental set up described in section 2.6.1. These values were compared with the pristine PCL membrane to determine the change in the permeability due to the presence of filler. Two types of experiments were performed: measurement of permeation of individual gases, and measurement of permeation of an equimolecular mixture.

It was necessary to determine the stabilization time of the system in which these gases were completely removed to ensure that the measurements made subsequently were only the chosen gas permeating through the membrane due to the possible contamination of module and pipes with atmospheric gases during the placement of the membranes. Therefore, a pristine PCL membrane was placed and left under a stream of 20 mL/min of O_2 as feed and 20 mL/min of He as sweep gas overnight measuring the permeated at intervals of 3 minutes. As can be seen in Figure 25, after 20-30 minutes no significant changes were observed in the permeation values. The same experiment was performed with CO_2 and a similar result was obtained (Figure 26).

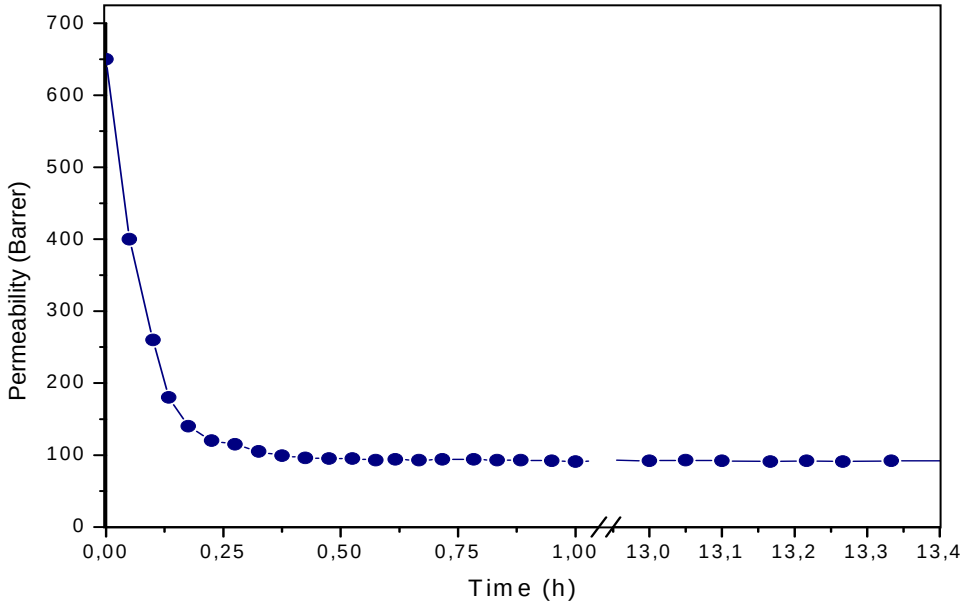

Figure 25. Stabilization time of a PCL membrane with O_2

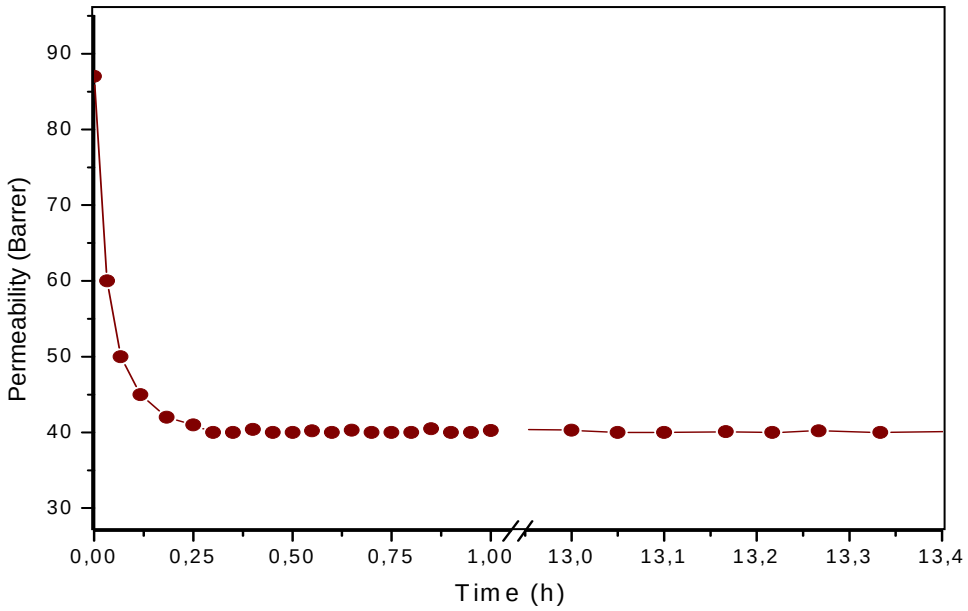

Figure 26. Stabilization time of a PCL membrane with CO_2

The individual gas permeation through pristine PCL membrane is shown in Figure 27 compared with the gas mixture at two different pressures. In both cases higher O_2 permeation was observed.

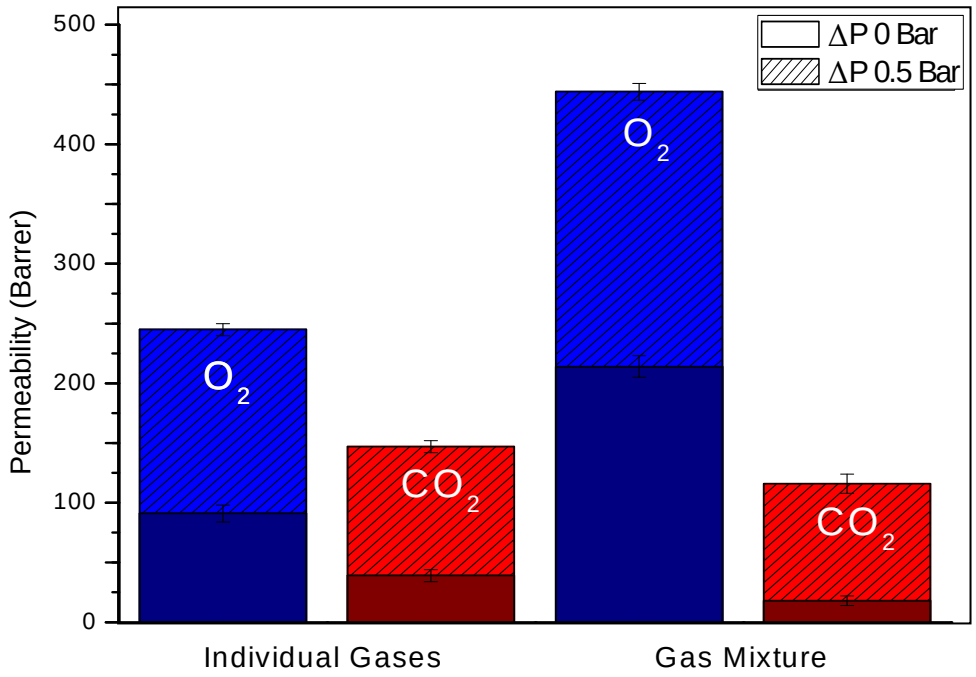

Figure 27. Permeation comparison between individual gases and mixtures through a PCL membrane

The permeation of gases through polymeric membranes usually occurs by two mean contributions: a dissolution phenomenon and a diffusion process across the membrane (solution-diffusion model). As a semi-crystalline polymer, polycaprolactone consists of an impermeable crystalline part, which will create a tortuous pathway through the membrane, and a permeable amorphous part where the solution and gas diffusion will occur. Furthermore, at 20 °C (temperature at which the experiments were carried out), the amorphous part of the polymer is in the rubbery state, in which the polymer chains have flexibility and mobility to allow the gas molecules diffuse through them **[16]**.

PCL shows high solubility for CO_2 due to two types of interactions: polar interactions between this gas and the ester groups of the polymer **[17]** and specific interactions (Lewis acid-base interactions) between CO_2 and oxygen of the carbonyl groups **[39]**. These interactions increase considerably the solution phenomenon, however diffusion is reduced. By contrast the O_2 barely interacts with the membrane, and its smaller kinetic diameter **[30]** favors diffusion through it. The higher permeation of oxygen would indicate that the solubility mechanism is not dominant in the transport of gases **[9]**.

Considering the permeation gas mixture, two differences were observed compared to individual gases: oxygen permeation is higher, and the CO_2 permeation is lower. These differences are due to the plasticizing effect of CO_2 **[40-42]**. Because of this effect, the CO_2 is capable of swelling the membrane, creating spaces between the polymer chains and thereby increasing the diffusion of O_2, and therefore the permeation. The decrease in the permeation of CO_2 may be due to the increase of the oxygen diffusion through the membrane. This gas could be capable of oxidizing groups in the polymer chains, promoting the interaction of CO_2 and thereby decreasing its permeation.

Finally, in all cases, increasing pressure an increase in permeation was observed. According Naito et al. **[43]** pressure in these polymers has two effects: one is due to the hydrostatic pressure that compresses the matrix, decreasing the movement of polymer chains and therefore the gas diffusion. The other effect is due to the dissolution of gas in the polymer. Considering that the amorphous zones of the polymer behaves like a liquid, the increment in pressure causes an increase in the dissolution of gas, which has

the effect of swelling the matrix (plasticizing) and thereby increases the permeation. By using low pressures (ΔP = 0.5 bar) the effect of the dissolution is dominant in these membranes considering the effect of hydrostatic pressure practically negligible. The effect of dissolution depends on the size of the molecule, for this reason, when the pressure increases, in both cases the oxygen permeation is higher.

In Figure 28 the individual gas permeation of pristine PCL and PCL composite membranes is shown.

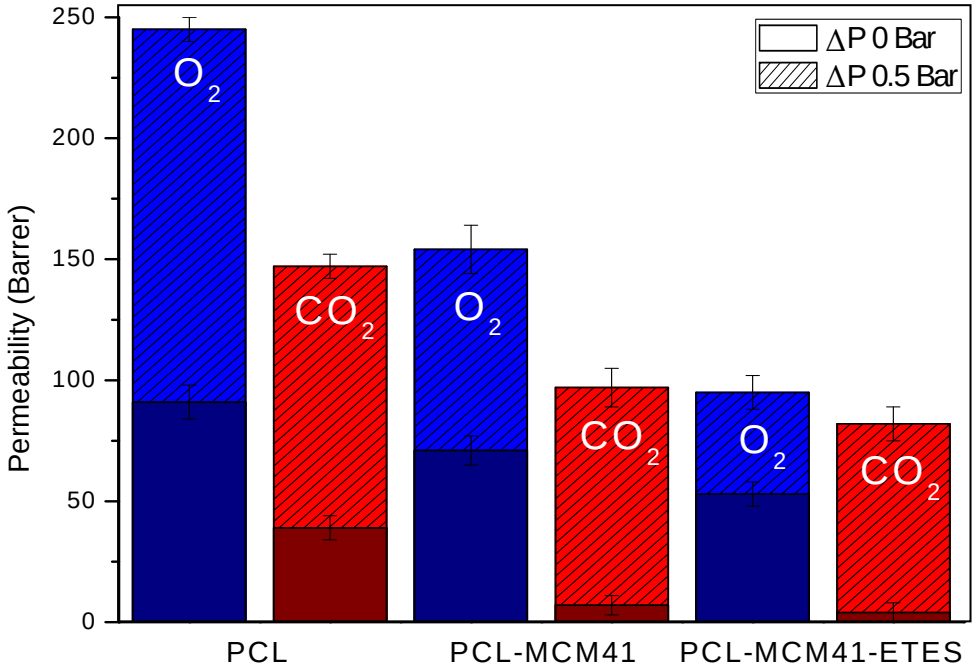

Figure 28. Permeation of membranes with individual gases

Comparing pristine PCL with PCL filled with MCM-41 a decrease in permeation is observed for both gases due to a set of phenomena. On the one hand, according to Sadeghi et al. **[9]**, in a semi crystalline polymer the silica is preferably to be placed into the amorphous zones. This breaks the packaging of the chains decreasing its flexibility and mobility, while increasing tortuosity, resulting in a decrease in the gas diffusion and thus a decreasing in the permeation.

On the other hand, due to in situ polymerization and taking into account that the cross sectional areas of polymeric chain are about 1 nm^2 or less, the polymer is able to penetrate into the pores of the silica during polymerization and increase the matrix-filler contact **[7]**. In the interior of the MCM-41 gas transport occurs through Knudsen

diffusion model, in which the permeation is inversely proportional to the molecular weight of the gases. The polymer penetration inside the silica makes larger pores inaccessible favoring the creation of a selective channels system for the diffusion of both gases **[6]**.

Both phenomena explain the decrease in permeation for both gases. For the O_2 a reduction in the permeation of 22 % is observed, compared to pristine PCL, while for the CO_2 permeation is reduced 82 % because of their larger molecular size which limits the diffusion of the gas through the mesoporous silica.

Finally, comparing the two membranes filled with MCM-41 can be observed a decrease in permeation of 25 % and 43 %, for O_2 and CO_2 respectively, in the membrane with the silica functionalized compared to the non-functionalized, and a decrease of 42 % and 90 % compared to the pristine PCL membrane. This reduction in permeation could be explained by interactions between the CO_2 and the amino groups of EPTES. According to Bacsik et al. **[38]**, sorbents modified with amines have a great capacity for chemisorption. In this research Bacsik proposes two reaction mechanisms, one fast (A) and another slow (B) as shown in Figure 29. Carbamic acids and ammonium carbamate are formed rapidly on contact with CO_2, reaction A. Furthermore, if the contact extends an additional ester is formed (silypropylcarbamate), reaction B. However this ester is not formed in the presence of water. Due to the hydrophilicity of our MCM-41, as seen in the section of FTIR, the interactions between CO_2 and amino groups of EPTES occur only through the reaction mechanism A.

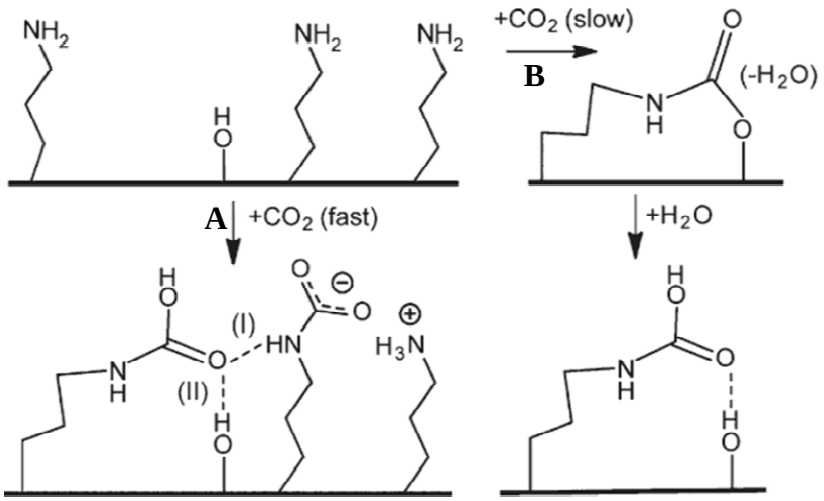

Figure 29. Proposed reaction mechanism between CO_2 and amino groups

Finally, in Figure 30 the values for the permeation of gas mixtures for the composite membrane are shown.

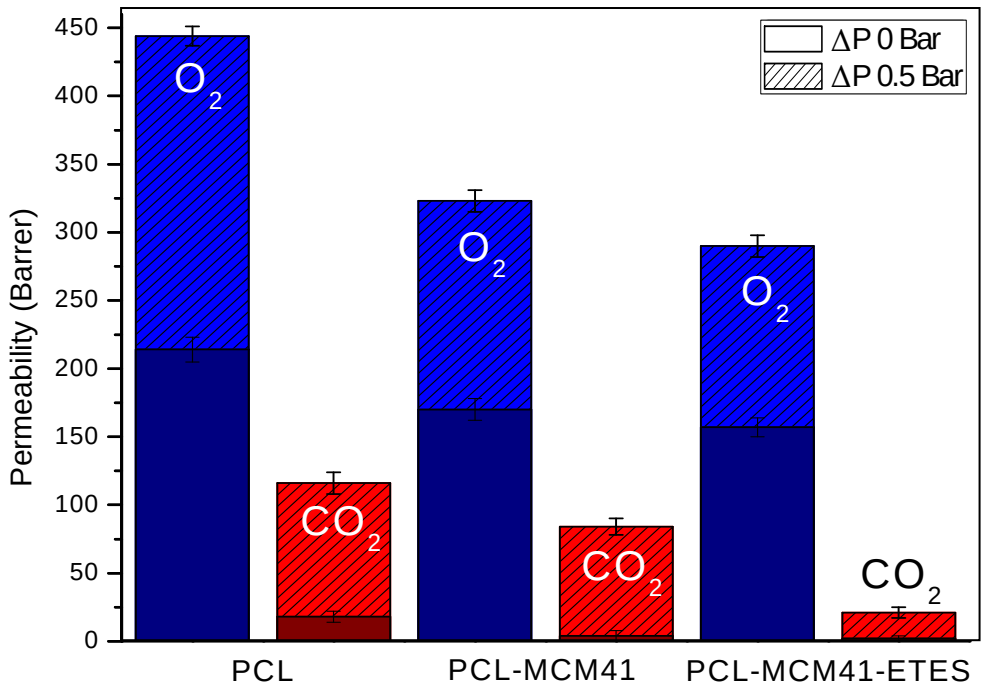

Figure 30. Permeation of membranes with a mixture of gases

As can be seen, the results are correlated. CO_2 interactions with ester and carbonyl groups of the polymer, besides it plasticizing effect, increase the permeation of O_2 in all cases compared to the individual gases.

The presence of MCM-41 and MCM-41 functionalized with EPTES decrease the permeation due to the same phenomena as in the individual gases, as explained above. Finally, the increment in pressure increases the permeation of the membranes due to the dilution effect discussed above.

Table 10 summarizes all the values obtained for the different permeation membranes.

Table 10. Permeation summary

Membrane	Pressure (Bar)	Individual Gases			Gas Mixture		
		Permeation		Ideal Selectivity	Permeation		Experimental Selectivity
		O2	CO2		O2	CO2	
PCL	0	91 ± 7	39 ± 5	2.33 ± 0.86	214 ± 9	18 ± 4	11.36 ± 1.86
	0.5	245 ± 5	147 ± 5	1.66 ± 0.39	444 ± 7	116 ± 8	3.85 ± 0.74
PCL-MCM41	0	71 ± 6	7 ± 4	10.58 ± 1.55	170 ± 8	4 ± 4	43.37 ± 2.01
	0.5	154 ± 9	97 ± 8	1.55 ± 0.30	323 ± 8	84 ± 6	3.82 ± 1.32
PCL-MCM41 EPTES	0	53 ± 5	4 ± 4	13.89 ± 1.82	157 ± 7	2 ± 2	80.21 ± 2.27
	0.5	95 ± 7	82 ± 7	1.21 ± 0.34	290 ± 8	21 ± 4	13.60 ± 1.93

In all cases a higher selectivity is observed in the gas mixture compared with the ideal selectivity obtained by the single gases. For individual gases the selectivity increases 4.5 and 6 times, for the case of PCL-MCM41 and PCL-MCM41-EPTES respectively, compared to pristine PCL membranes in experiments without overpressure. In experiments with an overpressure of 0.5 bar, selectivity decreases. This is due to the plasticizing effect of the CO_2 which, as explained above, increases the diffusion of both gases through the membrane.

Finally for the mixtures, the presence of MCM-41 increases the selectivity 3.8 times compared to pristine PCL, while in the case of work with 0.5 bar overpressure, the selectivity values were similar. However, the introduction of MCM-41 functionalized with EPTES increased selectivity 7 times, and 3.5 times with 0.5 bar overpressure respect to the pristine PCL, obtaining with these membranes the best selectivity results.

In view of these results, is possible to confirm that PCL membranes with MCM-41 as filler are capable of increasing the gas selectivity O_2/CO_2, compared to PCL membranes without filler.

5. Conclusions and Future Work

The presence of MCM-41 nanoparticles into PCL membranes results in an increment of O_2/CO_2 selectivity. In addition functionalization of these particles with EPTES increased considerably the selectivity, even working with an overpressure of 0.5 bar, making these membranes suitable for applications in which selective permeation is needed under atmospheric or under pressure conditions.

Also it should be noted that by solution casting and solvent evaporation method has been achieved to produce homogeneous membranes without defects, as has been seen by the different characterization techniques. Furthermore, this technique offers high reproducibility.

Future work on this project would involve:

- Use different concentrations of both MCM-41 and EPTES to find an optimum relation in which the selectivity is maximized.

- Conduct experiments on a wider range of pressures to study in detail the relationship between pressure and permeation.

- Carry out those experiments using other types of fillers in this PCL membrane to check if some improvement is achieved respect MCM-41.

References

[1] Cui, Z. F., & Muralidhara, H. S. (2010). Fundamentals of pressure-driven membrane separation process. In *Membrane Technology: A practical guide to membrane technology and applications in food and bioprocessing* (pp. 1-18). Burlington, MA: Elsevier.

[2] Paul, D. R., & Yampol´skii, Y. P. (1994). Introduction and perspective. In *Polymeric gas separation membranes* (pp. 1-16). New York, NY: CRC Press.

[3] Macanás, J. (2006). Desarrollo de nuevas membranas compuestas para la separación de iónes metálicos y aplicaciones electroquímicas (Doctoral Thesis). Universidad Autónoma de Barcelona, España.

[4] Baker, R. W. (2012). Overview of membrane science and technology. In *Membrane technology and applications*, 3rd Edition (pp. 1-16). Oxford, UK: Wiley.

[5] Guizard, C. (1999). Clasificación de las membranas y de los procesos que las utilizan (Master Thesis). Universidad de los Andes, Venezuela.

[6] Zornoza, B., et al. (2011). Mixed matrix membranes comprising glassy polymers and dispersed mesoporous silica spheres for gas separation. *Journal of Membrane Science*, 368, 100-109.

[7] Bento, A., et al. (2012). Gas permeability properties of decorated MCM-41/polyethylene hybrids prepared by in-situ polymerization. *Journal of Membrane Science*, 415-416, 702-711.

[8] Jomekian, A., et al. (2011). Gas transport behavior of novel modified MCM-48/polysulfone mixed matrix membrane coated by PDMS. *Journal of Membrane Science & Technology*, 1 (1).

[9] Sadeghi, M., et al. (2013). Preparation, characterization and gas permeation properties of a polycaprolactone based polyurethane-silica nanocomposites membrane. *Journal of Membrane Science*, 427, 21-29.

[10] Gorrasi, G., et al. (2003). Vapor barrier properties of polycaprolactone montmorillonite nanocomposties: effect of clay dispersion. *Polymer*, 44, 2271-2279.

[11] Cong, H., et al. (2007). Polymer-inorganic nanocomposites membranes for gas separation. *Separation and purification technology*, 55, 281-291.

[12] Mansourpanah, Y., et al. (2011). Fabrication new PES-based mixed matrix nanocomposites membranes using polycaprolactone modified carbon nanotubes as additive: Property changes and morphological studies. *Desalination*, 277, 171-177.

[13] Tian, D. et al. (1996). A new poly(ε-caprolactone) containing hybrid creamer prepared by the sol-gel process. *Polymer*, 37 (17), 3983-3987.

[14] Mark, J. E. (1991). Poly(ε-caprolactone). In *Polymer data handbook* (pp. 361-362). New York, NY: Oxford University Press.

[15] Tanaka, T., et al. (2006). Microfiltration membrane of polymer blend of poly(ι-lactic acid) and poly(ε-caprolactone). *Desalination*, 193, 367-374.

[16] Gain, O., et al. (2005). Gas barrier properties of poly(ε-caprolactone)/clay nanocomposites: influence of the morphology and polymer/clay interactions. *Journal of Polymer Science: Part B: Polymer Physics*, 43, 205-214.

[17] Cong, H., et al. (2007). Polymer-inorganic nanocomposites membranes for gas separation. *Separation and purification technology*, 55, 281-291.

[18] Lepoittevin, B., et al. (2002). Poly(ε-caprolactone)/clay nanocomposites prepared by melt intercalation: mechanical, thermal and rheological properties. *Polymer*, 43, 4017-4023.

[19] Cabedo, L., et al. (2006). Optimization of biodegradable nanocomposites based applications on a PLA/PCL blends for food packaging applications. *Macromolecular Symposium*, 223, 191-197.

[20] Sanchez-Garcia, M. D., et al. (2009). Development and characterization of novel biocomposites of thermoplastic biopolymers reinforced with carbon nanofiber and carbon nanotubes. 17th International Conference on Composite Materials, ICCM-17. Edinburgh, UK.

[21] Avella, M., et al. (2006). Poly(ε-caprolactone)-based nanocomposites: Influence of compatibilization on properties of poly(ε-caprolactone)-silica nanocomposites. *Composites Science and Technology*, 66, 886-894.

[22] Lee, E. J., et al. (2010). Nanostructured poly(ε-caprolactone)-silica xerogel fibrous membrane for guide bone regeneration. *Acta Biomaterialia*, 6, 3557-3565.

[23] Azeredo, H. (2009). Nanocomposites for food packaging applications. *Food Research International*, 42, 1240-1253.

[24] Tang, X. Z., et al. (2013). Recent advances in biopolymers and biopolymer-based nanocomposites for food packaging materials. *Critical Review in Food Science and Nutrition*, 52, 426-442.

[25] Wan, Y., et al. (2009). Thermophysical properties of polycaprolactone/chitosan blend membranes. *Thermochimica Acta*, 487, 33-38.

[26] Zeng, W., et al. (2005). Organic modified mesoporous MCM-41 through solvothermal process as drug delivery system. *Materials Research Bulletin*, 40, 766-772.

[27] López, L. Desarrollo de nanocomposites basados en poly(ε-caprolactona) (Doctoral Thesis pending publication). Universidad de Zaragoza, España.

[28] Tang, Z.G., et al. (2004). Surface properties and biocompatibility of solvent-cast poly[ε-caprolactone] films. *Biomaterials*, 25, 4741-4748.

[29] Stern, S.A. (1968). The "barrer" permeability unit. *Journal of Polymer Science Part A-2: Polymer Physics*, 6, 1933-1934.

[30] Yampolskii, Y., Pinnau, I., & Freeman, B. (2006). Transport of gases and vapors in glassy and rubbery polymers. In *Material science of membranes for gas and vapor separation* (pp. 1-47). Oxford, UK: Wiley.

[31] Liang, J.-Z. (2013). Reinforcement and quantitative description of inorganic particulate-filled polymer composites. *Composites: Part B*, 51, 224-232.

[32] Lucy, B., et al. (2007). Síntesis y caracterización de nanohíbridos poliestireno/sílica mesoporosa MCM-41. *Scientia et Technica Año XIII*, 36, 971-976.

[33] Elzein, T., et al. (2004). FTIR study of polycaprolactone chain organization at interfaces. *Journal of Colloid and Interface Science*, 273, 381–387.

[34] Zholobenko, V.L., et al. (1997). Synthesis of MCM-41 materials: an in situ FTIR study. *Microporous Materials*, 11, 83-86.

[35] Franco, R.L.M., et al. (2013). Textural properties of nickel, palladium and titanium oxides supported on MCM-41 materials and their application on oxidative desulfurization of dibenzothiophene. *Materials Research*, 16, 1448-1456.

[36] Grieken, R.V., et al. (2010). Sulfonated polystyrene-modified mesoporous silica for acid catalyzed processes. *Chemical Engineering Journal*, 161, 388-396.

[37] Li, S.Y., et al. (2013). 3-aminopropyltriethoxysilanes modified porous silicon as a voltammetric sensor for determination of silver ion. *International Journal of Electrochemical Science*, 8, 1802-1812.

[38] Bacsik, Z., et al. (2011). Mechanisms and kinetics for sorption of CO_2 on bicontinuous mesoporous silica modified with n-propylamine. *Langmuir*, 27, 11118-11128.

[39] Kazarian, S. G., et al. (1996). Specific intermolecular interaction of carbon dioxide with polymers. *Journal of the American Chemical Society*, 118, 1729-1736.

[40] Horn, N. R., et al. (2011). Carbon dioxide plasticization and conditioning effects in thick vs. thin glassy polymer films. *Polymer*, 52, 1619-1627.

[41] Minelli, M., et al. (2013). Permeability and solubility of carbon dioxide in different glassy polymer system with and without plasticization. *Journal of Membrane Science*, 444, 429-439.

[42] Neyertz, S., et al. (2014). The effect of structural isomerism on carbon dioxide sorption and plasticization at the interface of a glassy polymer membrane. *Journal of Membrane Science*, 460, 213-228.

[43] Naito, Y., et al. (1991). The effect of the pressure on gas permeation through semicrystalline polymers above the glass transition temperature. *Journal of Polymer Science: Part B: Polymer Physics*, 29, 457-462.